Inorganic Chemistry

Article

pubs.acs.org/IC

Influence of Tuned Linker Functionality on Modulation of Magnetic Properties and Relaxation Dynamics in a Family of Six Isotypic Ln_2 (Ln = Dy and Gd) Complexes

Soumya Mukherjee,[†] Jingjing Lu,[⊥,‡] Gunasekaran Velmurugan,[⊥,§] Shweta Singh,[†] Gopalan Rajaraman,*[,§] Jinkui Tang,*[,‡] and Sujit K. Ghosh*[,†]

[†]Indian Institute of Science Education and Research, Dr. Homi Bhabha Road, Pashan, Pune 411008, India

[‡]State Key Laboratory of Rare Earth Resource Utilization, Changchun Institute of Applied Chemistry, Chinese Academy of Sciences, Changchun 130022, P. R. China

[§]Department of Chemistry, Indian Institute of Technology Bombay, Powai, Mumbai, Maharashtra 400076, India

Supporting Information

ABSTRACT: A coordination complex family comprising of six new dinuclear symmetric lanthanide complexes, namely, $[Ln_2(L_x)_2(L')_2(CH_3OH)_2]\cdot yG$ (H_2L_x: three related yet distinct Schiff-base linkers; x = 1−3, according to the nomenclature of the Schiff-base linker employed herein. HL′: 2,6-dimethoxyphenol. yG refers to crystallographically assigned guest solvent species in the respective complexes; y = number of solvent molecules; Ln^{III} = Dy/Gd) were isolated employing a mixed-ligand strategy stemming out of a strategic variation of the functionalities introduced among the constituent Schiff-base linkers. The purposeful introduction of three diverse auxiliary groups with delicate differences in their electrostatic natures affects the local anisotropy and magnetic coupling of Ln^{III} ion-environment in the ensuing Ln_2 dinuclear complexes, consequentially resulting into distinctly dynamical magnetic behaviors among the investigated new-fangled family of isotypic Ln_2 complexes. Among the entire family, subtle alterations in the chemical moieties render two of the Dy_2 analogues to behave as single molecule magnets, while the other Dy_2 congener merely exhibits slow relaxation of the magnetization. The current observation marks one of the rare paradigms, wherein magnetic behavior modulation was achieved by virtue of the omnipresent influence of subtly tuned linker functionalities among the constituent motifs of the lanthanide nanomagnets. To rationalize the observed difference in the magnetic coupling, density functional theory and ab initio calculations (CASSCF/RASSI-SO/POLY_ANISO) were performed on all six complexes. Subtle difference in the bond angles leads to difference in the J values observed for Gd_2 complexes, while difference in the tunnel splitting associated with the structural alterations lead to variation in the magnetization blockade in the Dy_2 complexes.

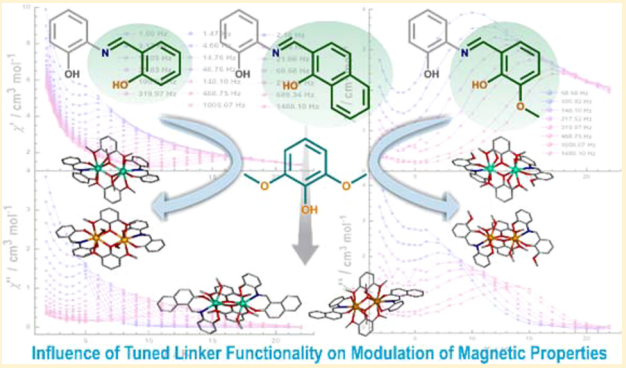

INTRODUCTION

The breakthrough revelation of single-molecule magnet (SMM) feature in Mn_{12} acetate complex[1−4] proved to be a giant quantum leap, since it triggered a rapid development behind exploring the different intriguing facets of magnetic properties for nanoscale magnetic coordination complex or cluster-based materials of varied nuclearity, over the span of last two decades.[5−11] SMMs are molecular species typically possessing the unmatched combination of high-spin (S) and uniaxial Ising-like magnetic anisotropy (D), leading to an anisotropy energy barrier (U) for the concomitant reversal of magnetization vector $S^2|D|$.[12−15] Majority of these efforts had been primarily aimed at the development of novel molecular magnets for miniaturizing devices in the nanoregime, involving the exciting facets of high-density information storage, quantum computing, and molecule spintronics.[16−24] Barring the initial focus that seemingly converged on polynuclear 3d metal aggregates, particularly large manganese clusters,[25−42] the following years until now have witnessed stupendous enthusiasm toward the development of mixed 3d−4f complexes as well as 4f-based lanthanide clusters.[13,15,43−65] Particularly, the attainment of maximum relaxation energy barrier and the highest blocking temperature for Ln(III)-based multinuclear clusters deserves special attention.[23,66−68] The crucial, rather imperative involvement of Ln(III) ions is to take advantage of the substantial magnetic anisotropy factor arising from the large unquenched orbital angular momentum of the constituent 4f metal ions, leading to an overall increase in the magnetic anisotropy value for the concerned complex and therefore,

Received: August 1, 2016

DOI: 10.1021/acs.inorgchem.6b01863
Inorg. Chem. XXXX, XXX, XXX−XXX

Scheme 1. Schematic Illustration of the Various Synthetic Schemes[a] Adopted to Obtain the Symmetric Ln_2 Family (Compounds 1a, 1b, 2a, 2b, 3a, and 3b)

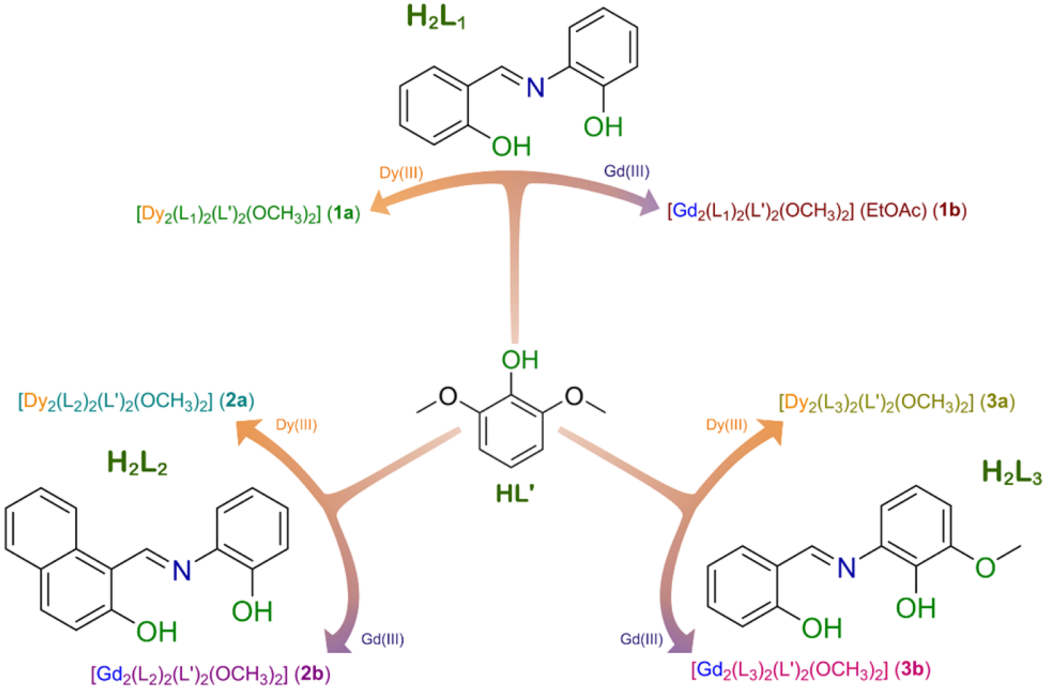

[a]On the basis of mixed-ligand-based strategy.

resulting in superior anisotropy energy barriers.[5,69−71] Hence, the well-adopted strategy to design and synthesize homometallic Ln(III) SMMs stems out of this favorable criterion of exploiting the high-anisotropy of 4f metal ions to utmost extent.[72−81] This is evident from the fact that hysteresis loop as high as 30 K are witnessed for seven coordinated Dy(III) SIMs.[82,83]

Intriguingly from a chemist's perspective, the intertwined interplay of the coordination geometry and ligand field effect coupled with the strength of magnetic interactions among the adjacent lanthanide sites along with the rational design of coordination chemistry assemblies' play as vital decisive factors behind the key route for synthesizing tailor-made functional SMMs. Moreover, Ln(III)-based SMMs hold the potential to come up with an exciting array of diverse quantum phenomena, such as thermally activated two-phonon or multiphonon magnetization relaxation and/or even magnetic tunneling,[84−90] which have already been comprehensively scrutinized in 3d SMMs. Keeping the focus pretty streamlined of acquiring a deeper insight into the structure−property correlations of magnetic coordination clusters pertaining to diverse nuclearity, a systematic synthetic approach is fundamentally essential to explicate the genesis of slow magnetic relaxation aimed at rational protocols of synthesizing better performing SMMs with high U and D values.[88−94] This culminated to the quite scarcely adopted mixed-ligand-based strategy[95−100] targeted at the development of quite a few related dysprosium-based SMMs, which could come up with noteworthy magnetic property variations based on subtle meteoric alterations in the electronic properties of the constituent linkers.[68,75,101−106]

Schiff-base linkers, especially the ones based on *o*-vanillin, are well-recognized to result into SMMs of varying nuclearity, since they can efficiently act as bridging linkers with a number of ligand-coordination pockets.[57,104−108] To employ three of such related multidentate Schiff-base bridging linkers, namely, H_2L_x (x = 1−3; Scheme 1), in conjugation with a typical chelating ligand, namely, 2,6-dimethoxyphenol (HL′), provides a unique mixed linker-based strategy for the systematic study of the magnetic modulation of a new dinuclear family of six symmetric Ln_2 (Ln = Dy and Gd) complexes based on subtle electronic changes of the constituent linkers. It is indeed mention-worthy that such comparative introspection of the constituent linkers' delicate electronic effects onto magnetic properties of the ensuing complexes, arising from strategic ligand-functionality tuning, has been rarely scrutinized among the miscellaneous spectra of SMM families.[109−112]

Herein, we report six dysprosium and gadolinium-based symmetric dinuclear compounds (Ln_2), namely, $[Dy_2(L_1)_2(L')_2(CH_3OH)_2]$ (**1a**), $[Gd_2(L_1)_2(L')_2(CH_3OH)_2]$-$(EtOAc)$ (**1b**), $[Dy_2(L_2)_2(L')_2(CH_3OH)_2]$ (**2a**), $[Gd_2(L_2)_2(L')_2(CH_3OH)_2]$ (**2b**), $[Dy_2(L_3)_2(L')_2(CH_3OH)_2]$ (**3a**), and $[Gd_2(L_3)_2(L')_2(CH_3OH)_2]$ (**3b**) (H_2L_1, H_2L_2, H_2L_3: as illustrated in Scheme 1, and HL′ = 2,6-dimethoxyphenol) by the designed variation principle of the participating Schiff-base linkers (Scheme 1), aimed at analyzing the outcomes of the delicate disparity between the closely related ligands onto the magnetic relaxation dynamics and characteristic properties for this family of six analogous molecular nanomagnets. As a distinct outcome of the aforesaid linker functionality-tuning among the three dissimilar yet closely related Schiff bases being employed (deprotonated ligand forms: L_1, L_2, and L_3, respectively), this report summarizes the distinct magnetic attributes of the new Ln_2 family comprising of six symmetric dinuclear clusters that are interrelated congeners, owing to the two sets of three Ln_2 clusters. Further, CASSCF/RASSI-SO/POLY_ANISO calculations were performed to gain insights into the mechanism of magnetic relaxation and the difference in the magnetic properties observed in this series.

DOI: 10.1021/acs.inorgchem.6b01863
Inorg. Chem. XXXX, XXX, XXX−XXX

Table 1. Crystallographic Data and Structure Refinement Details for the Ln_2 Family of Compounds 1a, 2a, 3a, 1b, 2b, and 3b

compound	1a	2a	3a	1b	2b	3b
empirical formula	$C_{44}H_{42}Dy_2N_2O_{12}$	$C_{54}H_{54}Dy_2N_2O_{14}$	$C_{46}H_{46}Dy_2N_2O_{14}$	$C_{48}H_{50}Gd_2N_4O_{14}$	$C_{52}H_{46}Gd_2N_2O_{12}$	$C_{46}H_{46}Gd_2N_2O_{14}$
formula wt	1117.79	1281.99	1177.85	1195.40	1207.41	1167.35
crystal system	monoclinic	monoclinic	orthorhombic	monoclinic	triclinic	orthorhombic
space group	$P2_1/n$	$P2_1/n$	*Pbca*	$P2_1/c$	$P\bar{1}$	*Pbca*
a, Å	8.6370(11)	8.895(4)	8.5275(15)	18.745(6)	8.5153(9)	8.601(2)
b, Å	14.4827(18)	12.546(6)	20.048(3)	15.930(5)	17.0101(19)	20.178(4)
c, Å	17.300(2)	22.112(10)	25.023(4)	18.388(6)	18.034(2)	25.138(5)
α (deg)	90.00	90.00	90.00	90.00	74.521(2)	90.00
β (deg)	101.278(2)	93.835(10)	90.00	119.316(7)	80.590(3)	90.00
γ (deg)	90.00	90.00	90.00	90.00	80.393(3)	90.00
V, Å^3	2122.3(5)	2462.2(19)	4277.9(12)	4787(3)	2462.6(5)	4362.7(17)
Z	2	2	4	4	2	4
ρ_{calc} g/cm^3	1.746	1.727	1.826	1.695	1.626	1.774
μ, mm^{-1}	3.559	3.083	3.539	2.817	2.733	3.085
temperature (K)	100	100	100	100	100	100
θ_{max} (deg)	28.41	28.202	26.373	28.629	28.160	28.301
F(000)	1096	1272	2320	2424	1192	2304
refl collected	20 924	22 743	27 474	48 316	39 582	21 960
independent refl	5306	5988	4343	11 985	11 846	5410
GOF	1.708	0.896	1.051	1.008	1.192	0.794
final *R* indices [$I > 2\sigma(I)$]	R_1 = 0.0309 wR_2 = 0.0550	R_1 = 0.0363 wR_2 = 0.1021	R_1 = 0.0556, wR_2 = 0.1141	R_1 = 0.0346, wR_2 = 0.0651	R_1 = 0.0458, wR_2 = 0.1530	R_1 = 0.0397, wR_2 = 0.1041
R indices (all data)	R_1 = 0.0506, wR_2 = 0.0571	R_1 = 0.0418 wR_2 = 0.1154	R_1 = 0.0985, wR_2 = 0.1329	R_1 = 0.0575, wR_2 = 0.0738	R_1 = 0.0712, wR_2 = 0.1752	R_1 = 0.0663, wR_2 = 0.1238

EXPERIMENTAL SECTION

Materials and Measurements. All the reagents and solvents were commercially available and used without further purification. Fourier transform IR spectra were measured on NICOLET 6700 FT-IR Spectro-photometer using KBr Pellets. Thermogravimetric analyses were obtained in the temperature range of 30−800 °C on PerkinElmer STA 6000 analyzer under a N_2 atmosphere at a heating rate of 10 °C min.

X-ray Structural Studies. Single-crystal X-ray data for all the six Ln_2 compounds (**1a**, **2a**, **3a**, **1b**, **2b**, and **3b**, respectively; see Table 1) were collected at 100 K on a Bruker KAPPA APEX II CCD Duo diffractometer (operated at 1500 W power: 50 kV, 30 mA) using graphite-monochromated Mo Kα radiation (λ = 0.710 73 Å), mounting on nylon CryoLoops (Hampton Research) with mineral oil (Paraton-N, Hampton Research). The data integration and reduction were processed with SAINT[113] software. A multiscan absorption correction was applied to the collected reflections. The structures were solved by the direct method using SHELXTL[114] and were refined on F^2 by full-matrix least-squares technique using the SHELXL-97[115] program package within the WINGX[116] program. All non-hydrogen atoms were refined anisotropically. All hydrogen atoms were located in successive difference Fourier maps, and they were treated as riding atoms using SHELXL default parameters. The structures were examined using the *Adsym* subroutine of PLATON[117] to ensure that no additional symmetry could be applied to the models. Tables S1−S6 contain the complete crystallographic data set for these compounds. CCDC Nos. 1420355, 1420356, 1420357, 1420358, 1420359, and 1420360 (**1a**, **1b**, **2a**, **2b**, **3a**, and **3b**, respectively) contain the supplementary crystallographic data for these compounds. Additional crystallographic information is available following the Supporting Information. X-ray powder patterns were recorded on Bruker D8 Advanced X-ray diffractometer at room temperature using Cu Kα radiation (λ= 1.5406 Å).

Synthesis of Linker H_2L_1. The Schiff-base ligand 2-((2-hydroxybenzylidene)amino)phenol (L_1H_2) was synthesized via a slightly modified synthetic protocol from the ones reported in the literature.[118−121] *o*-Aminophenol (10.9 g, 100 mmol) was heated under reflux conditions with salicylaldehyde (12.2 g, 100 mmol) in a 120 mL binary solvent mixture of toluene and ethanol (7:5, v/v) for 0.5 h, following which the reaction solution was cooled over an ice−salt bath, which yielded bright reddish-yellow crystals of H_2L_1. The highly crystalline product, once washed well with hot EtOH, was dried first in open atmosphere and then under vacuum; subsequently, it was used for further complexation-mediated syntheses, yield 17.89 g (~92%). ^{1}H NMR (400 MHz, acetone-d_6; Figure S4): δ 8.9 (s, 1H); 8.6 (S, 1H), 7.6 (dd, *J* = 7.2, 1.2 Hz, 1H), 7.4 (m, 1H), 7.3 (dd, *J* = 8.0, 1.2 Hz, 1H), 7.15 (m, 1H), 6.9 (m, 4H); ^{13}C NMR (100 MHz, acetone-d_6; Figure S7): δ 206.3, 163.9, 162.1, 151.9, 137.0, 133.7, 128.9, 121.1, 120.7, 119.7, 117.7; high-resolution mass spectrometry (HRMS; electrospray ionization (ESI); Figure S1): Calcd for $C_{13}H_{11}NO_2$ $[M + H]^+$: 214.0868; Found: 214.0868. Elemental Analysis: Anal. Calcd for $C_{13}H_{11}NO_2$: C, 73.23; H, 5.20; N, 6.57. Found: C, 73.49; H, 5.14; N, 6.71%.

Synthesis of Linker H_2L_2. Similar procedure (as for H_2L_1) was also employed to synthesize linker 2-(((2-hydroxyphenyl)imino)-methyl)naphthalen-1-ol (H_2L_2); the only alteration being the use of equimolar 2-hydroxy-1-naphthaldehyde in place of salicylaldehyde;[122] yield 20.39 g (~85%). ^{1}H NMR (400 MHz, deuterated dimethyl sulfoxide (DMSO-d_6); Figure S5): δ 15.7 (d, *J* = 9.6 Hz, 1H), 10.3 (s, 1H), 8.4 (d, *J* = 8.0 Hz, 1H), 7.9 (dd, *J* = 8.0, 1.6 Hz, 1H), 7.8 (d, *J* = 9.2 Hz, 1H), 7.7 (dd, *J* = 7.6, 1.6 Hz, 1H), 7.5 (m, 1H), 7.3 (m, 1H), 7.1 (m, 1H), 7.0 (dd, *J* = 8.0, 1.2 Hz, 1H), 6.9 (m, 1H), 6.8 (d, *J* = 9.2 Hz, 1H); ^{13}C NMR (100 MHz, DMSO-d_6; Figure S8): δ 177.3, 149.5, 148.4, 137.8, 133.8, 128.9, 128.6, 128.0, 126.7, 125.8, 125.0, 123.0, 119.8, 119.6, 117.6, 115.9, 107.7; HRMS (ESI; Figure S2): Calcd for $C_{17}H_{13}NO_2$ $[M + H]^+$: 264.1024; Found: 264.1027. Elemental Analysis: Anal. Calcd for $C_{17}H_{13}NO_2$: C, 77.55; H, 4.98; N, 5.32. Found: C, 77.84; H, 5.82; N, 5.26%.

Synthesis of Linker H_2L_3. Similar synthetic protocol (as described for H_2L_1) was followed for linker 2-((2-hydroxybenzylidene)amino)-6-methoxyphenol (H_2L_3); the single essential change being the replacement of salicylaldehyde by equimolar *o*-vanillin;[123,124] yield 20.94 g (~94%). ^{1}H NMR (400 MHz, acetone-d_6; Figure S6): δ 8.1 (s, 1H); 7.8 (s, 1H), 6.5 (dd, *J* = 8.4, 2.8 Hz, 1H), 6.4 (m, 1H), 6.34 (m, 1H), 6.29 (dd, *J* = 7.6, 1.2 Hz, 1H), 6.2 (dd, *J* = 8.0, 1.2 Hz, 1H), 6.1 (dd, *J* = 7.6, 1.2 Hz, 1H), 6.0 (m, 1H), 3.1 (s, 1H); ^{13}C NMR (100 MHz, acetone-d_6; Figure S9): δ 206.3, 163.7, 152.7, 151.9, 149.5, 136.9, 128.9, 124.9, 121.2, 120.7, 119.2, 117.4, 116.45, 56.6; HRMS (ESI; Figure S3): Calcd for $C_{14}H_{13}NO_3$ $[M + H]^+$: 244.0973; Found:

DOI: 10.1021/acs.inorgchem.6b01863
Inorg. Chem. XXXX, XXX, XXX−XXX

244.0977. Elemental Analysis: Anal. Calcd for $C_{14}H_{13}NO_3$: C, 69.12; H, 5.39; N, 5.76. Found: C, 68.93; H, 5.37; N, 5.91%.

Synthesis of $[Dy_2(L_1)_2(L')_2(CH_3OH)_2]$ (1a). A methanolic solution of H_2L_1 (21.3 mg, 0.1 mmol in 5 mL) and HL′ (15.4 mg, 0.1 mmol) was deprotonated with triethylamine (41.5 μL, 0.3 mmol), to which solid dysprosium nitrate hydrate (45.7 mg, 0.1 mmol) was added, along with 5 mL of ethyl acetate (EtOAc). This reaction mixture was kept in undisturbed conditions at room temperature. Yellow single crystals of compound **1a** suitable for single-crystal X-ray analysis were obtained after slow evaporation of the binary solvent mixture of MeOH/EtOAc over a span of just 10 h (overnight). ∼62% yield (based on metal). IR (KBr, cm^{-1}): 1894 (vw), 1597 (m), 1473 (s), 1308 (s), 1169 (w), 1088 (m), 1007 (w), 918 (w), 837 (m), 737 (s), 563 (vw). Anal. Calcd (found) for compound **1a** ($C_{44}H_{42}Dy_2N_2O_{12}$): C, 47.36 (47.64); N, 2.51 (2.69); H, 3.79 (3.38)%.

Synthesis of $[Gd_2(L_1)_2(L')_2(CH_3OH)_2]$(EtOAc) (1b). Pale brown single crystals of compound **1b**, suitable for X-ray diffraction analysis, were obtained; the synthetic protocol being similar (identical molar ratios for the respective reactants involved) to the reaction for synthesizing **1a**. ∼59% yield. IR (KBr, cm^{-1}): 1778 (vw), 1593 (m), 1470 (w), 1304 (s), 1169 (vw), 1091 (m), 1007 (w), 930 (vw), 837 (m), 741 (s), 563 (w). Anal. Calcd (found) for compound **1b** ($C_{48}H_{50}Gd_2N_4O_{14}$): C, 47.20 (46.98); N, 4.59 (4.88); H, 4.13 (4.07)%.

Synthesis of $[Dy_2(L_2)_2(L')_2(CH_3OH)_2]$ (2a). A methanolic solution of H_2L_2 (26.3 mg, 0.1 mmol in 3 mL) and HL′ (15.4 mg, 0.1 mmol) was deprotonated with triethylamine (41.5 μL, 0.3 mmol), to which solid dysprosium nitrate hydrate (45.7 mg, 0.1 mmol) was added, along with 7 mL of EtOAc. The homogeneous solution was kept uninterrupted at room temperature, as yellow platelike crystals of compound **2a** suitable for single-crystal X-ray analysis emerged on slow evaporation of the binary solvent mixture of MeOH/EtOAc just within 4 h. ∼71% yield. IR (KBr, cm^{-1}): 1724 (w), 1597 (s), 1470 (m), 1381 (m), 1277 (s), 1092 (m), 1011 (vw), 837 (s), 741 (s), 552 (m). Anal. Calcd (found) for compound **2a** ($C_{54}H_{54}Dy_2N_2O_{14}$): C, 50.67 (51.10); N, 2.19 (2.31); H, 4.25 (4.89)%.

Synthesis of $[Gd_2(L_2)_2(L')_2(CH_3OH)_2]$ (2b). Dark red single crystals of compound **2b**, suitable for X-ray diffraction analysis, were formed from an analogous reaction as the one for synthesizing **2a**. ∼64% yield. IR (KBr, cm^{-1}): 1905 (vw), 1724 (w), 1601 (m), 1485 (m), 1385 (s), 1281 (m), 1169 (w), 1092 (m), 1007 (vw), 837 (m), 725 (s), 552 (w). Anal. Calcd (found) for compound **2b** ($C_{52}H_{46}Gd_2N_2O_{12}$): C, 51.81 (51.03); N, 2.32 (2.45); H, 3.85 (3.51)%.

Synthesis of $[Dy_2(L_3)_2(L')_2(CH_3OH)_2]$ (3a). A methanolic solution of H_2L_3 (24.3 mg, 0.1 mmol in 3 mL) and HL′ (15.4 mg, 0.1 mmol) was deprotonated with triethylamine (41.5 μL, 0.3 mmol), to which solid dysprosium nitrate hydrate (45.7 mg, 0.1 mmol) was added, along with 7 mL of EtOAc. This reaction mixture was kept in undisturbed conditions at room temperature, as yellow single crystals of compound **3a**, suitable for X-ray diffraction analysis, were obtained after slow evaporation of the binary solvent mixture of MeOH/EtOAc over a span of just 6 h. ∼66% yield. IR (KBr, cm^{-1}): 1878 (vw), 1732 (m), 1612 (m), 1473 (m), 1385 (vw), 1311 (w), 1173 (vw), 1092 (w), 968 (w), 849 (s), 725 (s), 555 (w). Anal. Calcd (found) for compound **3a** ($C_{46}H_{46}Dy_2N_2O_{14}$): C, 46.99 (46.68); N, 2.38 (2.44); H, 3.94 (3.78)%.

Synthesis of $[Gd_2(L_3)_2(L')_2(CH_3OH)_2]$ (3b). Bright red single crystals of compound **3b**, suitable for X-ray diffraction analysis, were derived from an analogous reaction as the one for synthesizing **3a**. ∼69% yield. IR (KBr, cm^{-1}): 1855 (vw), 1728 (m), 1601 (s), 1385 (m), 1470 (m), 1308 (m), 1092 (s), 952 (vw), 849 (m), 725 (s), 552 (w). Anal. Calcd (found) for compound **3b** ($C_{46}H_{46}Gd_2N_2O_{14}$): C, 47.41 (47.09); N, 2.40 (2.46); H, 3.9 (3.99)%.

Magnetic Measurement (Experimental) Details. All magnetization data were recorded on a Quantum Design MPMS-XL7 SQUID magnetometer. The variable-temperature magnetization was measured with an external magnetic field of 1000 Oe in the temperature range of 1.9−300 K. Diamagnetic corrections for the bulk phase-pure polycrystalline compounds were estimated from the Pascal's constants,[125] and magnetic data were corrected for diamagnetic contributions of the sample holder.

Computational Details. To compute the *g*-tensors and the energies of Kramers doublet the ab initio calculations were performed on the complexes using MOLCAS 7.8 quantum chemistry package.[126−129] In this multiconfigurational approach, relativistic approach was treated based on Douglas−Kroll Hamiltonian. We employed atomic natural (ANO-RCC) basis set for the calculations of *g*-tensor. The following contraction schemes were employed [8s7p5d3f2g1h] for Dy, [4s3p2d1f] for N, [4s3p2d1f] for O, 3s2p] for C, and [2s] for H. The ground-state atomic multiplicity of Dy^{III} is $^6H_{15/2}$, which result in eight low-lying Kramers doublets. The CASSCF calculation comprises an active space of nine active electrons in the seven active orbitals (CAS (9,7)). In CASSCF calculation active space (9,7) is adopted, and hence, 21 sextets were considered. In the last step we used SINGLE_ANISO code[130] implemented in the MOLCAS to compute the *g*-tensors of Dy^{III} ions.

To further account for the exchange interaction between the metal sites using the above acquired lowest spin−orbit states, Lines model[131] was used. The Lines model has been proved to be useful owing to its intrinsic single parameter (*J*) consideration, which corresponds to an effective isotropic magnetic exchange interaction.[53,132−134] The Lines exchange coupling followed by the estimation of magnetic properties of the dinuclear complex were undertaken using the POLY_ANISO program,[135−137] interfaced with the SINGLE_ANISO module. The resultant exchange spectrum and correlated wave functions of the dinuclear complexes were used to determine temperature and field-dependent magnetic properties of the dinuclear complexes.

Density Functional Theory Calculations. Density functional calculations were performed for complexes **1b−3b** using the B3LYP functional,[138] with the G09 code.[139] We used the double-ζ quality basis set employing Cundari-Stevens[140] (CSDZ) relativistic effective core potential on Gd atom, TZV basis set[141] for the rest of the atoms. The density functional theory (DFT) calculations combined with the broken symmetry (BS) approach were employed to estimate exchange constant between the Gd^{III}−Gd^{III} ions. This computational approach is proven to be reliable for computing exchange coupling constants in Gd(III) complexes.[142,143] The simulation of magnetic susceptibility data (**1b−3b**) is obtained using PHI software.[144] DFT calculations on complexes **1a−3a** were performed using ORCA software.[145] In ORCA, BS-DFT[146] calculations, we employed B3LYP functional conjunction with SARC−DKH[147−149] basis set for Dy and TZVP for rest of the elements.

RESULTS AND DISCUSSION

All the aforementioned six compounds' family (**1a**, **1b**, **1c**, **2a**, **2b**, and **2c**) were prepared at room temperature by slow evaporation of the respective low-boiling reaction solvent mixtures like MeOH or EtOAc. Single-crystal X-ray analysis technique was employed to indisputably determine the structures for all of them. With the salicylaldehyde-based Schiff-base linker L_1 in unison with the new-fangled bridging ligand L′, the compounds **1a** and **1b** got crystallized in monolinic space groups $P2_1/n$ and $P2_1/c$, with $Z = 2$ and $Z = 4$, respectively; the more conjugated naphthalene-based linker L_2-derived analogous compounds **2a** and **2b** crystallized in monoclinic and triclinic space groups $P2_1/n$ ($Z = 2$) and $P\bar{1}$ ($Z = 2$), respectively. As a correlated finding, the ubiquitously used *o*-vanillin-based ligand L_3 led to the formation of compounds **3a** and **3b**, both endowed with the orthorhombic crystallographic space group *Pbca*.

The molecular structures of compounds **1a** and **1b** (with partial labeling), presenting the symmetric dinuclear core, is shown in Figure 1, while the similar ones for compounds **2a−2b** and **3a−3b** are illustrated in Figures 2 and 3, respectively. The compound **1a** is composed of two crystallographically unique Dy1 atoms bridged by two μ_2-oxo (O4) bridges from

DOI: 10.1021/acs.inorgchem.6b01863
Inorg. Chem. XXXX, XXX, XXX−XXX

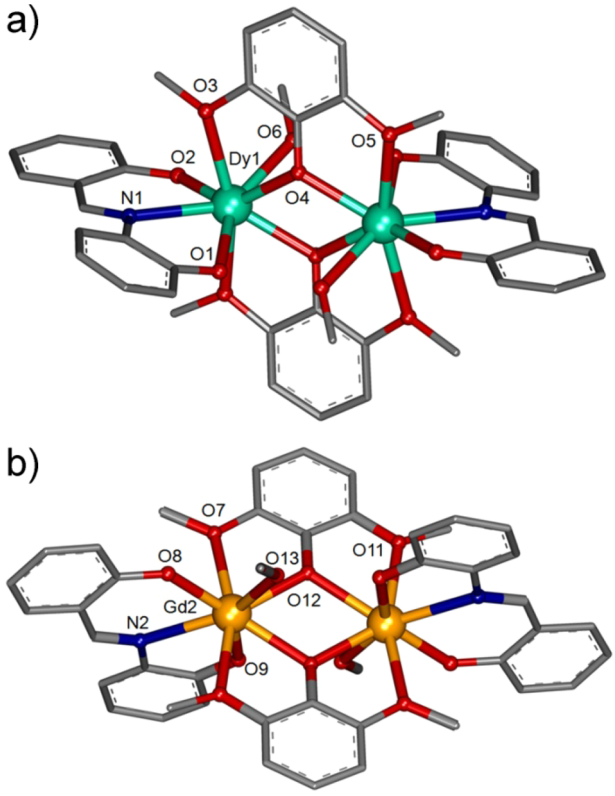

Figure 1. Partially labeled molecular structures of complexes (a) **1a** and (b) **1b**, harnessed from the mixed-ligand strategy approach adopted herein. Hydrogen atoms and solvent molecules were omitted for clarity.

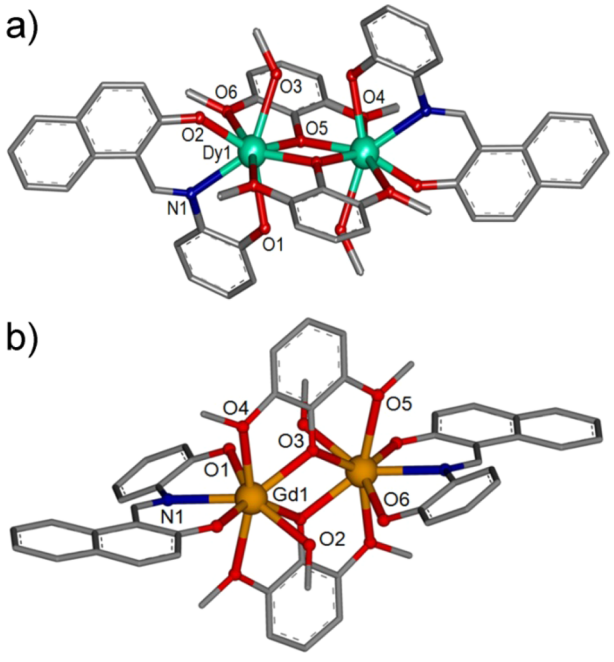

Figure 2. Partially labeled molecular structures of complexes (a) **2a** and (b) **2b**, stemming out of the mixed-ligand strategy approach followed herein. Hydrogen atoms and solvent molecules were omitted for clarity.

the two L′ linkers, which also coordinates in bidentate fashion via O5 and O3 centers. Considering deprotonated form of the κ^3 Schiff-base L_1, two O-centers O2 and O1, along with N1

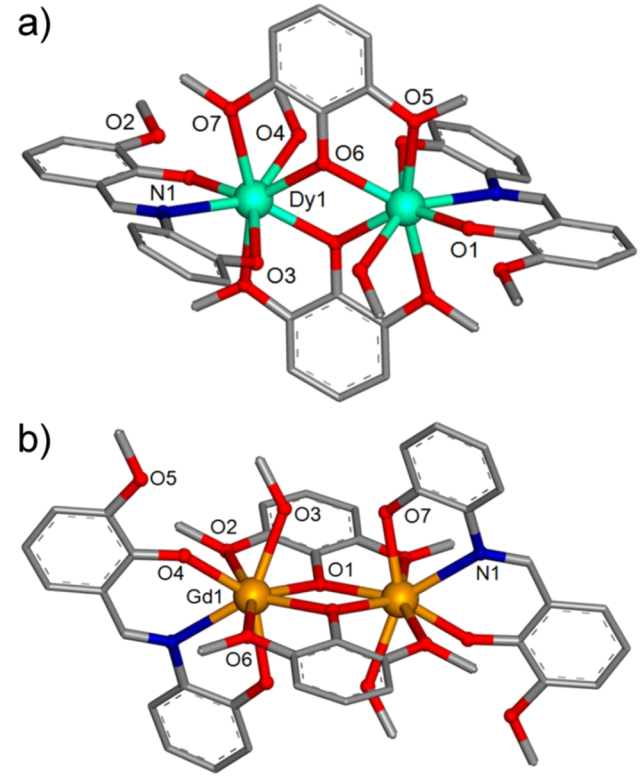

Figure 3. Partially labeled molecular structures of complexes (a) **3a** and (b) **3b**, developed by virtue of the mixed-ligand strategy of employing H_2L_3 and HL′ both. Hydrogen atoms and solvent molecules were omitted for clarity.

center, coordinate to each of the two Dy-centers. On the one hand, two methanol molecules coordinating via O6 satisfy the octacoordination environment for each of the Dy(III) centers. On the other hand, compound **1b** (adopted space group: $P2_1/c$) composed of exactly same set of units; coordinating ligands assembles with Gd(III) to crystallize in two crystallographically unique, but structurally similar, Gd_2; consequently (see Table S18), only one is considered in the ensuing discussion. The O4, N1, and O6 atoms of the tridentate Schiff-base L_1 coordinate to each of the crystallographically identical Gd1 centers; O5 and O1 centers of the L′ ligand act as the ones from an apposite capping ligand, while simultaneously bridging the Gd1 centers via O2 center. For the other crystallographically distinct core comprising of Gd2 pair, centers O8, O9, and N2 serve as the chelating centers from the Schiff base L_1, alongside O7, O11 centers capping the two Gd2 centers' coordination spheres held by a bridging μ_2-oxo center (O13). The intermetallic distances among the two Ln_2 centers (two pairs of Gd1 and Gd2) in the symmetric complex **1b** are nearly similar: 3.899 and 3.887 Å, respectively, being comparable to that in the single Dy_2 core of **1a**, 3.833 Å. The Dy−O−Dy bond angles in compounds **1a** and **1b** are 111.12° (Dy1−O4−Dy1) and 111.87° (Gd2−O12−Gd2), 112.97° (Gd2−O12−Gd2), respectively.

The molecular architectures of Ln_2 compounds **2a** and **2b** (with requisite labeling) is shown in Figure 2, while the similar ones for compounds **3a** and **3b** are exhibited in Figure 3. The compound **2a** is constituted from two crystallographically distinctive Dy1 atoms bridged by two μ_2-oxo (O5) bridges stemming out of the two L′ linkers, which also involves bidentate coordination via O6 and O4 centers. The analogous ligating centers for compound **2b** composed of two crystallo-

DOI: 10.1021/acs.inorgchem.6b01863
Inorg. Chem. XXXX, XXX, XXX−XXX

graphically distinguishable Gd_2 units are μ_2-oxo (O11), O8, O10 (for Gd2 center) and μ_2-oxo (O3), O4, O5 (for Gd1 center). While O2, N1, and O1 atoms of the two coordination pocket-containing imine ligand L_2 coordinate to the Dy(III) centers, the pairs of O9, N2, O7 (Gd2) and O1, N1, O6 (Gd1) enjoy favorable ligation to the Gd(III) centers in **2b**. Terminal methanol molecules coordinating via O3 (Dy1 in **2a**), O12 (for Gd2 in **2b**), and O2 (via Gd1 in **2b**) fulfill the eightfold square antiprismatic coordination geometry adopted by each of the Ln(III) centers in case of this related pair. The interlanthanide distance between the two metal centers for the Dy(III) complex **2a** being 3.831 Å, is evidently quite close to the ones observed for the double core-complex **2b**: 3.851 Å (Gd2) and 3.837 Å (Gd1), respectively. The Dy1−O5−Dy1 bond angle of 111.52° observed in compound **2a** (Dy1−O4−Dy1) analogously has a proximity to the 110.79° (Gd2−O11−Gd2) and 110.43° (Gd1−O3−Gd1), respectively, observed for complex **2b**.

The isotypic compounds **3a** and **3b** constituted from two sets of crystallographically unique Ln1 (Ln = Dy and Gd for **3a** and **3b**, respectively) atoms, which are similarly bridged by two μ_2-oxo (O6 and O1, respectively) bridges arising from the respective L′ linkers (see Table S18). This pair also engages bidentate coordination of L′ via the combination of O5, O7 and O6, O2 paired centers (for compounds **3a** and **3b**, respectively). Interestingly enough, tridentate ligand L_3 possesses three coordination pockets, unlike the double-containing ones realized in its previously discussed congeners L_1 and L_2, owing to the presence of chelating methoxy moiety (O2 and O5 for **3a** and **3b**, respectively) in ortho position to the chelating hydroxyl group therein. Unlike literature reports of this linker utilizing its all three coordination pockets for complexation with 4f ions,[92] this compound's architecture presents only tridentate coordination of L_3, merely exploiting its two imine bond-adjacent pockets. The ligating centers of Schiff-base L_3 for compounds **3a** and **3b** are O1, N1, O3 and O4, N1, O7, respectively; leading to two symmetric Ln_2 structures with Dy−Dy and Gd−Gd distances of 3.837 and 3.859 Å alongside Dy1−O6−Dy1 angle assuming 111.60° and a proximally anticipated Gd1−O1−Gd1 angle of 110.81°. The square antiprismatic geometry for all the Dy and Gd centers are requisitely completed by the linked methanol molecules donating via O4 to Dy1 (in **3a**) and O3 to Gd2 (in **3b**).

Considering all the six complexes, apart from the μ^2-η^2:η^2 bridged L′ spacer, the coordination modes adopted by the constituent analogous Schiff-base ligands are precisely matching (Figure S20). In addition to the anticipated η^3 binding mode assumed by L_1 and L_2, ligand L_2 in spite of possessing one additional chelating pocket prefers to bind via the same η^3 coordination mode to the lone Ln(III) centers on each of the vertices of the Ln_2 architecture leading to the exact resemblance of the linker binding modes. Thermogravimetric analysis data recorded for all these six isotypic compounds (Supporting Information, Figures S16 and S17) show significant thermal stability up to nearly 155 °C with almost no weight loss, corresponding to the absence of any guest molecule in all the air-dried phases of this dinuclear family. Powder X-ray diffraction studies for all the six compounds (**1a**, **1b**, **2a**, **2b**, **3a**, and **3b**) reveal highly crystalline characteristic profiles signifying phase purity for each of the discussed series of coordination complexes. As discussed in the aforementioned discussion highlighting the coordination environment features for the Ln_2 family, the anticipated variation of the interlanthanide distances and the metal−ligand−metal nodal angles is indeed observed, owing to the strategically introduced manipulation in the Schiff-linker environment of the tuned linker functionality. This might play as one of the crucial contributing factors behind the ensuing exhibition of considerable alterations in their magnetic properties.

The systematic analysis on the coordination geometry was performed using SHAPE software[150] on the octacoordinated lanthanide ions of all the complexes. The results reveal that all the complexes are found to be intermediate geometry between square antiprism (D_{4d}) and dodecahedron (D_{2d}; Tables S17 and S18). The slight deviation was observed within Gd(III) and Dy(III) analogues due to the various substituents. Within a complex both the Gd(III) and Dy(III) centers show similar values, which clearly indicates that both the centers are highly symmetry. All the Dy(III) complexes (**1a**−**3a**) show similar values due to its isotypic environment.

Direct-current (dc) magnetic susceptibility studies of **1a**−**3b** were performed in an applied magnetic field of 1 kOe over the temperature range of 2−300 K. The plots of $\chi_M T$ versus T, where χ_M is the molar magnetic susceptibility, are shown in Figure 4. The observed $\chi_M T$ products at 300 K for all

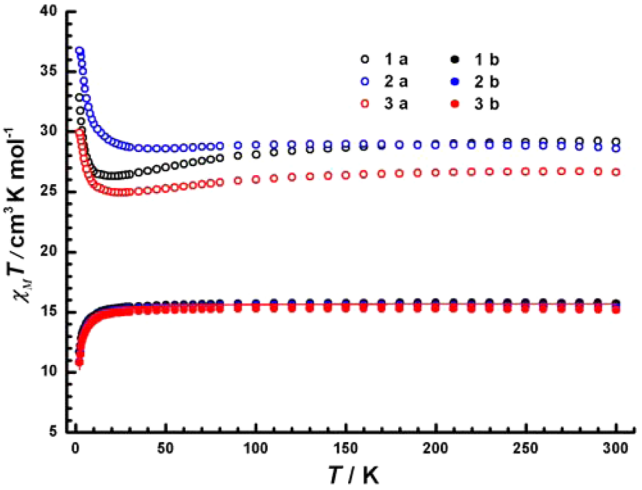

Figure 4. Temperature dependence of $\chi_M T$ products at 1 kOe for **1a**−**3b**. The solid red lines are best fits as described in the text.

compounds are almost in good agreement with the expected value for two uncoupled lanthanide ions. When cooled, however, the $\chi_M T$ values show different tendency, which is dependent on lanthanide ion. Herein, we classify the compounds based on lanthanide ions to describe the magnetic properties.

For complexes **1a** and 2a, the $\chi_M T$ values at 300 K are 29.15 and 28.57 cm^3 K·mol^{-1}, respectively, which is in agreement with the expected value of 28.36 cm^3 K·mol^{-1} for two uncoupled Dy^{III} ions ($^6H_{15/2}$, J = 15/2, g = 4/3). But the $\chi_M T$ value of 26.62 for **3a** at 300 K is slightly smaller than the theoretical value due to the splitting of the $^6H_{15/2}$ ground state.[151−154] The $\chi_M T$ products gradually decrease with lowering temperature, reaching a minimum value of 26.29, 28.59, and 25.93 cm^3 K·mol^{-1} at ∼40 K, which is mainly ascribed to the depopulation of the Stark sublevels and/or significant magnetic anisotropy present in Dy systems.[155] The $\chi_M T$ value then increases sharply to a maximum of 32.85, 36.75, and 29.91 cm^3 K·mol^{-1} at 2 K for **1a**, **2a**, and **3a**, respectively, indicating the presence of weak intramolecular ferromagnetic

DOI: 10.1021/acs.inorgchem.6b01863
Inorg. Chem. XXXX, XXX, XXX−XXX

interactions between Dy^{III} spin carriers as observed in other dysprosium systems.[104,156] The field-dependent magnetizations for all compounds are shown in Figures S21−S29. For **1a**, **2a**, and **3a**, the magnetization rises abruptly at low fields and reaches 11.60, 15.64, and 10.10 μ_B at 7 T, without saturation (Figure S21−S23). This suggests the presence of magnetic anisotropy and/or the considerable crystal-field effects.[157] The non-superposition of the M versus H/T data (Figure S27−S29) also suggests the presence of significant magnetic anisotropy and/or low-lying excited states.

With the replacement of Dy^{III} ions with Gd^{III} ions, analogous compounds **1b**, **2b**, and **3b** are isolated. The $\chi_M T$ products at room temperature are close to the expected value for two uncoupled Gd^{III} ions. As the temperature is lowered, the $\chi_M T$ product remains constant until 30 K, at which point $\chi_M T$ monotonically decreases, ultimately reaching 11.70, 10.87, and 10.81 $cm^3\ K{\cdot}mol^{-1}$ at 2 K. To evaluate the coupling parameters, the expression[153]

$$\hat{H} = -J\cdot\hat{S}_A\cdot\hat{S}_B + \beta(\hat{S}_A\cdot g_A + \hat{S}_B\cdot g_B)\cdot\hat{H}_Z$$

is applied on compounds **1b**−**3b** with $S = 7/2$. The fits for compounds **1b**−**3b** give $J = -0.07(9)$, $-0.09(2)$, and $-0.09(7)$ cm^{-1}, respectively. This negative J confirms the antiferromagnetic interaction is very weak between the Gd^{III} centers. The field-dependent magnetization approximate to the expected values for two isolated Gd^{III} ions without saturation (Figures S24−S26) suggests the presence of the considerable crystal-field effects.[157]

In view of the SMM behavior, alternating-current (ac) susceptibility measurements were also performed under zero dc fields for **1a**, **2a**, and **3a** (Figures 5, 6, and S30). Temperature-dependent in-phase (χ') and out-of-phase (χ'') magnetic susceptibility signals for **1a** exhibit a peak at 14 K; when cooled, a new peak tail of χ' and χ'' is observed below 5 K (Figure 6a). Frequency-dependent susceptibility data were collected in the range of 1−1500 Hz under zero applied dc field. As shown in Figure 5a, the maximum values of χ'' were temperature-dependent between 4.5 and 13 K over the entire frequency range. This indicates that the relaxation does not cross over to a pure mechanism of quantum tunneling mechanism (QTM) at temperatures above 4.5 K, contrary to what is often observed for the majority of Ln^{III}-based SMMs, where the QTM is fast.[99,158]

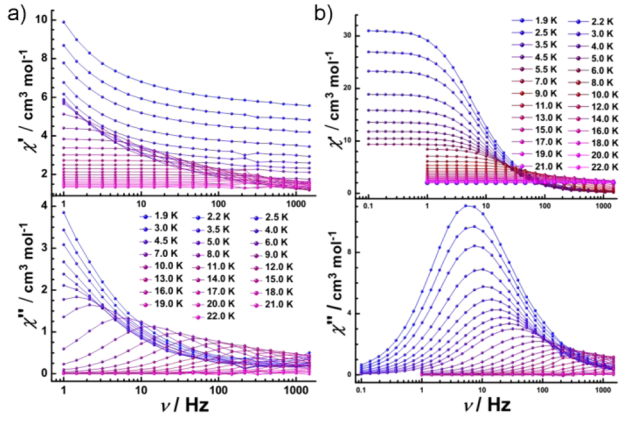

Figure 5. Frequency-dependent ac susceptibility for **1a** (left) and **2a** (right) in the absence of a static field.

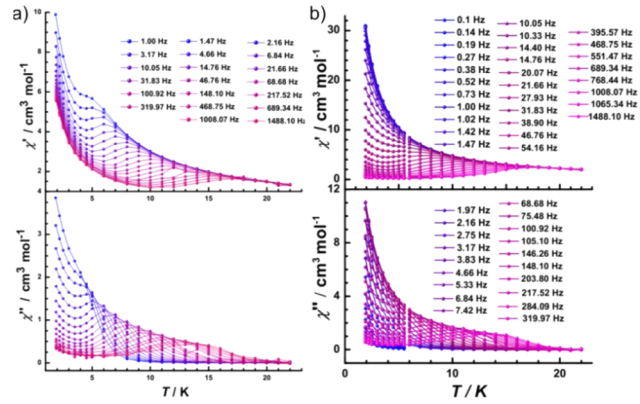

Figure 6. (a) Temperature-dependent ac susceptibility for (a) **1a** and (b) **2a** in the absence of a static field.

Similar SMM behavior can be observed in **2a**, which exhibits a peak at 12 K and rapid increase below 5 K (Figure 6b). The rapid increase in the low-temperature region could be attributed to quantum tunneling effect at zero dc field. The χ'' peaks show a frequency dependence in the high-temperature region, signaling the relaxation of the spins through the anisotropy barrier. When decreasing the temperature, the maxima of the out-of-phase χ'' peaks shift toward lower frequency until 3 K, then maintain in the same frequency, confirming the classic quantum regime. Meanwhile, an increase in the χ'' component observed again in the low-temperature region is also typical of the onset of tunneling relaxation.[71] From the one set of peaks $\chi''(\upsilon)$ curves, we can see that the thermally activated spin reversal is gradually replaced at low temperature by a tunneling relaxation mechanism (Figure 5b).

To study the magnetic process, Cole−Cole plots of χ'' versus χ' (Figure 7a,b for **1a** and **2a**, respectively) were constructed and fitted to a generalized Debye model to determine α values and relaxation times τ in the temperature ranges of 8−14 and 6−22 K for **1a** and **2a**, respectively. The plots reveal relatively symmetrical semicircles, indicating a single relaxation process, with α values in the ranges of 0.10−0.16 and 0.08−0.24 for **1a** and **2a**, respectively, indicating a broad distribution of relaxation times. On the basis of the ac susceptibility analysis, a higher energy can be expected for **1a** compared to **2a** because of the relatively weak tunneling of magnetization in **1a**. To further investigate this prediction, the energy barriers were evaluated with fitting to the Arrhenius law (Figure 8). The magnetization relaxation time τ was extracted from the maxima

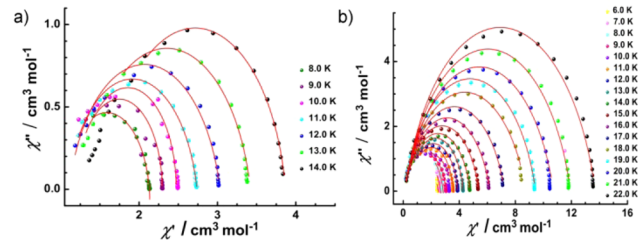

Figure 7. (a) Cole−Cole plots for complex **1a** between 8 and 14 K; the solid lines are the best fits to the experimental data, obtained with the generalized Debye model with α parameters in the range of 0.10−0.16. (b) Cole−Cole plots for complex **2a** between 6 and 22 K; the solid lines are the best fits to the experimental data, obtained with the generalized Debye model with α parameters in the range of 0.09−0.24.

DOI: 10.1021/acs.inorgchem.6b01863
Inorg. Chem. XXXX, XXX, XXX−XXX

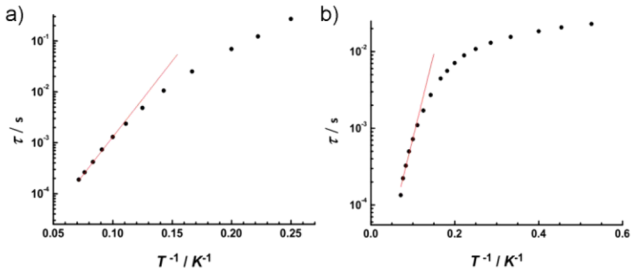

Figure 8. Magnetization relaxation time constant τ vs T^{-1} for **1a** (left) and **2a** (right) in a zero static field from best fit to the Arrhenius law of the thermally activated regime (solid line).

of the out-of-phase peaks. The best fits yield effective energy barriers of U_{eff} = 69 K with pre-exponential factor $\tau_0 = 1.37 \times 10^{-6}$ s, and U_{eff} = 51 K with $\tau_0 = 4.54 \times 10^{-6}$ s for **1a** and **2a**, respectively. The barrier of compound **2a** seems to be smaller compared with that of **1a** as a result of the faster quantum tunneling.

The dynamics of magnetization for **3a** were also investigated from ac susceptibility measurements, in a zero static field at the indicated frequencies given in Figure 9a. The χ'' component of

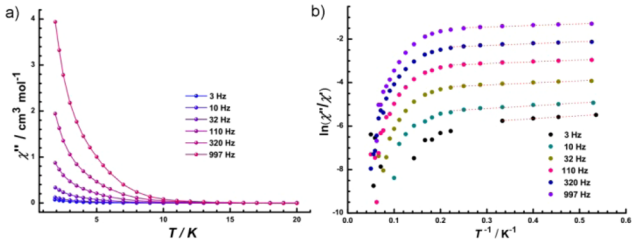

Figure 9. (a) Temperature dependence of the out-of phase ac susceptibility for **3a** in the absence of a static field. (b) Natural logarithm of the ratio of χ'' over χ' vs $1/T$ of the data for **3a** given in Figure 9a. Slope corresponding to energy barrier U_{eff} = 1.0 K.

the susceptibility has a strong frequency dependence below 8 K to the lowest measured temperature of 1.9 K, indicating the onset of the slow magnetization (M) relaxation expected for SMM behavior.

Although the expected maximum due to blocking could not be observed down to this temperature, a method[159] assuming that there is only one characteristic relaxation process of the Debye type with one energy barrier and one time constant. With this assumption, one can evaluate roughly the energy barrier and τ_0 based on the following relationship (eq):

$$\ln(\chi''/\chi') = \ln(\omega\tau_o) + U_{eff}/kT$$

This methodology had been applied earlier in the determination of τ_0 in Mn_{12} acetate[160] and U_{eff} and τ_0 in Fe_3Ln. As shown in Figure 9b, by fitting the experimental χ''/χ'' data to eq, the parameter values $U_{eff} \approx 1.0$ K and $\tau_0 \approx 1 \times 10^{-4}$ s were obtained. A more precise result must wait for very low-temperature measurements (T < 1 K) by using a micro-SQUID.

Theoretical Studies. To gain further insight into the mechanism of magnetic relaxation and to rationalize the difference in the observed magnetic behavior we performed ab initio and DFT calculations for the complexes **1a**−**3a** and **1b**−**3b**, respectively.

To evaluate exchange parameter and their relationship between the structures, the DFT studies were performed on the complexes **1b**−**3b**. The DFT-computed J values are found to be −0.034 cm^{-1} (**1b**), −0.054 cm^{-1} (**2b**), and −0.049 cm^{-1} (**3b**; see Table S8 in Supporting Information). All the complexes found to exhibit weak anti-ferromagnetic exchange interactions due to weak overlap between the 4f orbitals. The computed J values are in agreement with the experimental estimate, and it reproduces not only the sign of J but also their magnitude and the trends. The magnitude of J shows the presence of weak exchange interactions as evidenced in other [Gd^{III}−Gd^{III}] complexes.[142] The comparison of experimental and calculated magnetic susceptibility (simulated based on the DFT J values) for complexes **1b**−**3b** are shown in Figure 10. It

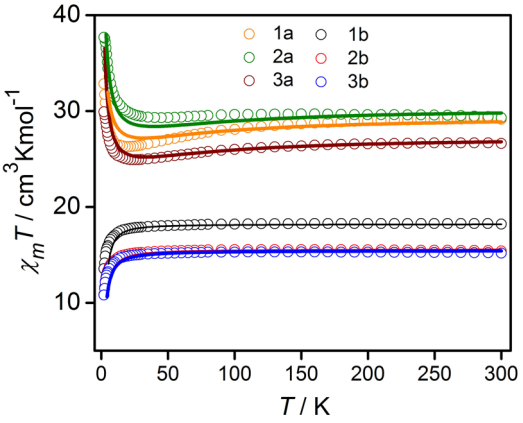

Figure 10. A comparison of the experimental and calculated (solid line) magnetic susceptibility for complexes **1a**−**3b**.

clearly demonstrates that the simulation of the magnetic properties with the computed exchange constants reproduces the magnetic susceptibility exactly. Among the three complexes, complex **1b** is found to less anti-ferromagnetic than complexes **2b** and **3b**, and this is correlated to relatively large Gd−O−Gd angles found in complex **1b** compared to complexes **2b** and **3b** (average Gd−O−Gd angles are 112.4°, 110.6°, and 110.8° for complexes **1b**, **2b**, and **3b**, respectively). This is consistent with the Gd−O−Gd magneto−structural correlation proposed.[142]

To understand the mechanism of magnetic coupling, the computed spin densities are analyzed. The net J value has contributions from ferromagnetic part and anti-ferromagnetic parts, and the sign of exchange is decided by the dominating factor. As per our earlier mechanism of magnetic exchange for {Gd−Gd} pair, the anti-ferromagnetic contributions arise from the overlap between the 4f orbitals, while the polarization by the 4f orbitals to the empty 5d/6s/6p shells contribute to ferromagnetic coupling.[142] Relatively larger Gd−O−Gd angles estimated for complexes **1b**−**3b**, and the low symmetric nature leads to significant overlap between the 4f orbital pairs. This contribute significantly for the anti-ferromagnetic part of the exchange leading to negative Js in all three complexes. The computed spin densities for complex **1b** is shown in Figure 11 (S = 0 state; for complexes **2b** and **3b** see Figure S32 of Supporting Information). The spin densities of Gd^{III} ion (~7.02 for both) show the presence of spin polarization, as the 4f orbitals are deeply buried. It is noteworthy that spin delocalization is poor is due to the contracted nature of 4f orbitals, whereas spin polarization is exceeded leading to opposite spin densities on the atoms connected to Gd. Eventually the bridging oxygen atoms are having more spin densities (due to polarization of the both Gd atoms) than other

DOI: 10.1021/acs.inorgchem.6b01863
Inorg. Chem. XXXX, XXX, XXX−XXX

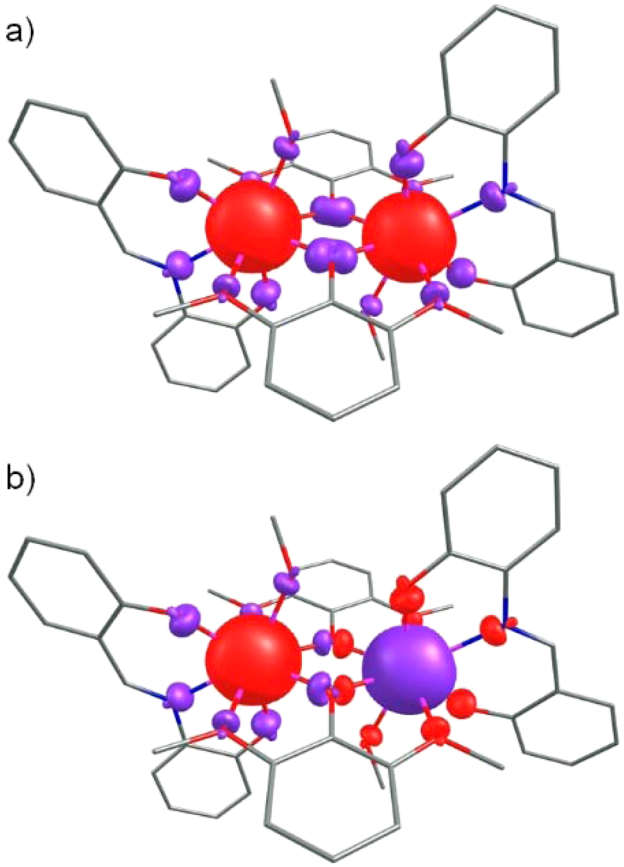

Figure 11. Spin density plot of the complex **1b** (a) high spin and (b) broken symmetry shown with isosurface values of 0.001 Å^{-3}.

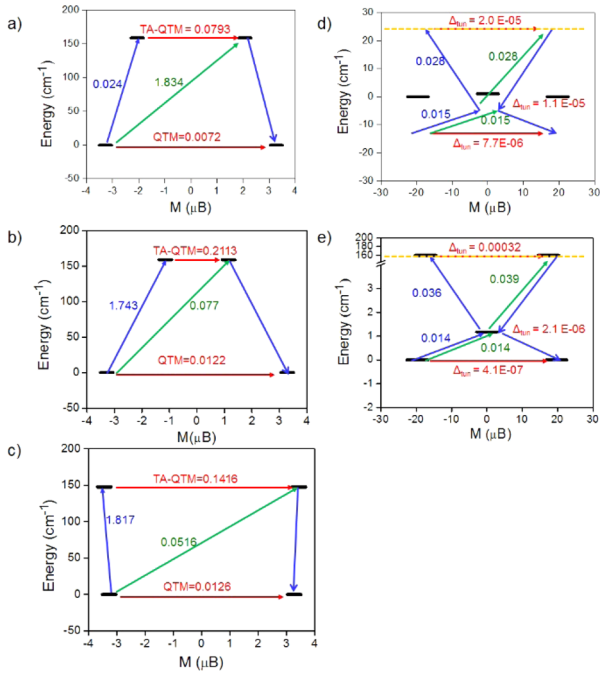

Figure 12. (a−c) Ab initio SINGLE_ANISO computed magnetization blocking barrier for **1a−3a**. The thick black lines imply the Kramers doublet as a function of magnetic moment. The green lines indicate the possible pathway of the Orbach (Raman) contribution of magnetic relaxation. The blue lines show the most suitable relaxation pathway for magnetization reorientation. The red lines correspond to the QTM/TA-QTM of relaxation contribution between the connecting pairs. The black texts near the black lines reveal the nature of the KDs in terms of major wave function contribution. (d, e) Ab initio POLY_ANISO computed low-lying exchange spectrum and position of the magnetization blocking barrier (yellow dashed line) for **1a−3a**. Here, the thick black lines represent exchange-coupled energy levels, while the solid lines signify similar description as for SINGLE_ANISO results. Here the red lines indicate tunnel splitting within the exchange-coupled states of the exchange spectrum.

atoms, and this favors the weak anti-ferromagnetic coupling as reported in our earlier studies.[142]

To understand the mechanism of magnetic relaxation in Dy(III) complexes, ab initio CASSCF calculations are performed. The qualitative mechanism of magnetic relaxation of the uncoupled Dy(III) single ion corresponding to complexes **1a−3a** are shown in Figures 12a−c. Here, the *x*-axis indicates the magnetic moment of each state along main magnetic axis, while *y*-axis denotes the energy of the respective states. The numbers shown in Figure are the mean absolute values of the matrix elements of the magnetic moment. The energy of each Kramers doublet (KD) on each individual Dy(III) ion is given in Tables S12−S14 in Supporting Information. The large value of g_{zz} (g_{zz} = 20) reveals the presence of large magnetic moment, approaching that expected for a pure m_J = ±15/2 state.[161] It was observed that QTM is suppressed in all the cases due to the pure Ising nature of the ground-state anisotropy. As shown in Table S10, the energy spectrum of the states arising from the ground-state free ion differs in **1a−3a**. The large energy separation between the ground and excited doublet is observed in all the cases.

Significant tunneling at the excited KDs suggest TA-QTM via first excited state to be operational for magnetic relaxation, and this suggests the barrier heights of 159, 159, and 147 cm^{-1} for complexes **1a−3a**, respectively. These values are much higher than the estimated U_{eff} values. This may be due to the computational limitation of not considering intermolecular interactions and QTM between the ground-state KDs.[162] The same was observed in the literature that the energy difference observed is clear indication of several relaxation pathways other than Orbach process. In addition, the overestimated excitation energies of the local Dy(III) multiplets, as obtained in CASSCF approximation, might also be one of the reasons.[163]

The crystal-field parameters were investigated for better understanding of the relaxation mechanism (Table S15). Interestingly, the major part of the ligand-field effect comes from both axial and nonaxial parameters. The two Dy(IIII) ions experience symmetric ligand field, which is evident in the local anisotropy axes. The nearly equal strength of the axial and nonaxial terms suggests that it will not relax via ground-state KD but via the first excited KD.

To further understand the mechanism of magnetic relaxation, dinuclear Dy(III) relaxation mechanism diagrams are constructed using POLY_ANISO program employing Lines model. Within the dimer, dipolar interaction between the Dy(III) centers were calculated and given in the Table 2. With the Lines parameter, the simulated susceptibility (J_{Dy-Dy}) for complex **1a−3a** are −0.090, 0.13, and −0.097 cm^{-1}, respectively. This yielded a reasonable fit to the experimental data for complexes **1a−3a** as shown in Figure 10 (total coupling parameter J_{tot}). Interestingly, for complex **2b** calculations yield ferromagnetic coupling, while **1a** and **3a** are estimated to be anti-ferromagnetically coupled. As the experimental susceptibility obtained is slightly higher than the calculated one, a scaling factor of 6−8% for the calculated

DOI: 10.1021/acs.inorgchem.6b01863
Inorg. Chem. XXXX, XXX, XXX−XXX

Table 2. Exchange and Dipolar Interactions and Computed Anisotropic *g*-Tensor Values (g_{xx}, g_{yy}, and g_{zz}) Obtained from POLY_ANISO Calculation for Complexes 1a−3a [cm^{-1}]

interaction	1a		2a		3a	
dipolar	0.180		0.200		0.194	
exchange	−0.090		0.130		−0.097	
total	0.090		0.330		0.097	
doublet	g_{xx}	Δ_{tun}	g_{xx}	Δ_{tun}	g_{xx}	Δ_{tun}
	g_{yy}		g_{yy}		g_{yy}	
	g_{zz}		g_{zz}		g_{zz}	
1	0.00	7.7×10^{-06}	0.00	4.1×10^{-07}	0.00	2.0×10^{-05}
	0.00		0.00		0.00	
	39.31		39.39		39.26	
2	0.00	1.1×10^{-05}	0.00	2.1×10^{-06}	0.00	3.1×10^{-05}
	0.00		0.00		0.00	
	0.023		0.040		0.026	
3	0.00	2.0×10^{-05}	0.00	0.000 32	0.00	0.000 11
	0.00		0.00		0.00	
	36.11		35.60		35.75	
4	0.00	0.000 20	0.00	0.000 34	0.00	0.000 60
	0.00		0.00		0.00	
	36.10		35.60		35.74	
5	0.00	0.000 17	0.00	0.000 36	0.00	0.000 57
	0.00		0.00		0.00	
	0.013		0.900		0.002	
6	0.00	0.000 11	0.00	0.000 29	0.00	0.000 33
	0.00		0.00		0.00	
	0.028		0.889		0.003	

curves are required. This may be attributed to the loss of solvation, as possible evaporation of coordinate/uncoordinated solvent molecules are not often accounted for corrections. The estimated exchange interaction is smaller than that of the dipolar magnetic coupling; as the result, exchange and dipolar parts are not stabilizing the nonmagnetic state. The Dy−Dy axes slightly favor the strong dipolar magnetic interaction and thus the parallel arrangement of the local magnetic axes arises. To validate the computed exchange parameter, we computed the Dy^{III}−Dy^{III} exchange using broken symmetry DFT approach implemented in Orca software. The result reveals that the calculated *Js* values are in agreement with the *J* exchange obtained from POLY_ANISO program. The established mechanism of magnetic relaxation for the dinuclear systems is in agreement with the dynamic magnetic susceptibility data measured. Besides the difference in the observed barrier heights are found to be correlated to the structural alterations.

The calculated local magnetic moments in the ground exchange doublet state and the main magnetic anisotropy axis are shown in Figures 12 and Figure 13, respectively. Because of the symmetric nature the orientation of the local magnetic anisotropy axes and magnetic moments are parallel to each other. The orientation of the principle anisotropy axes of the Dy(III) ions are perpendicular to the two bridging ligands. And it lies close to the Dy−O bonds as expected. The *g*-tensor for all the Dy(III) ions are mostly Ising type (Tables S12−S14). For complexes **1a**−**3a**, six exchange Ising doublets are obtained from six lowest-lying KDs on the two Dy(III) sites (Table S16, Figure 12d,e). The exchange states in Figure 12d,e are arranged in compliance with their corresponding maximal magnetic moments. The lowest exchange levels were grouped into doublets, and these doublets are split by tunnel splitting (Δ_{tun}) as indicated. For all the exchange-coupled states, the transverse components are found to be nearly zero ($g_{xx} = g_{yy} = 0 < 1 \times 10^{-9}$), and orientation of the magnetic anisotropy of the ground state resembles that of the Dy(III) single-ion behavior. However, the tunnel splitting (Δ_{tu}) for the ground state is estimated to be different with values larger than 7.7×10^{-6} cm^{-1} estimated for complexes **1a** and **2a**, while relatively larger tunnelling splitting observed for complex **3a** (2×10^{-5} cm^{-1}), suggesting possible ground-state tunnelling for this complex.[164,165] This suggests relaxation of magnetization for complexes **1a** and **2a** via the third excited KD placing the estimate of U_{cal} as 159 and 160 cm^{-1} for complexes **1a** and **2a**, respectively.

Relatively larger tunnelling at the ground state for complex **3a** suggests meager barrier height, and this is consistent with the experimental estimates. The estimated barrier heights for complexes **1a** and **2a** are however much larger than the experimental estimate, and this may be attributed to the fact that in the estimation of U_{cal} value other effects such as intermolecular interaction/hyperfine interaction/non-Orbach mechanisms are not taken into consideration.[53,137,162,163,166,167,167] Although the differences are marginal, slightly larger tunnelling gap for complex **3b** observed is due to small difference in the structural parameters leading to enhanced transverse anisotropy and larger tunnelling gap at the coupled Dy(III) states. This suggests the importance of fine-tuning the barrier height by employing different ligand architecture.

CONCLUSION

On a closing note to this report, a new family of dinuclear and symmetric lanthanide complexes, comprising of six congeners, which have been assembled by adopting a mixed-ligand strategy based on three minutely altered linkers with small yet distinct changes in one particular constituent ligand functionality's electronic nature. DFT was employed to rationalize the

DOI: 10.1021/acs.inorgchem.6b01863
Inorg. Chem. XXXX, XXX, XXX−XXX

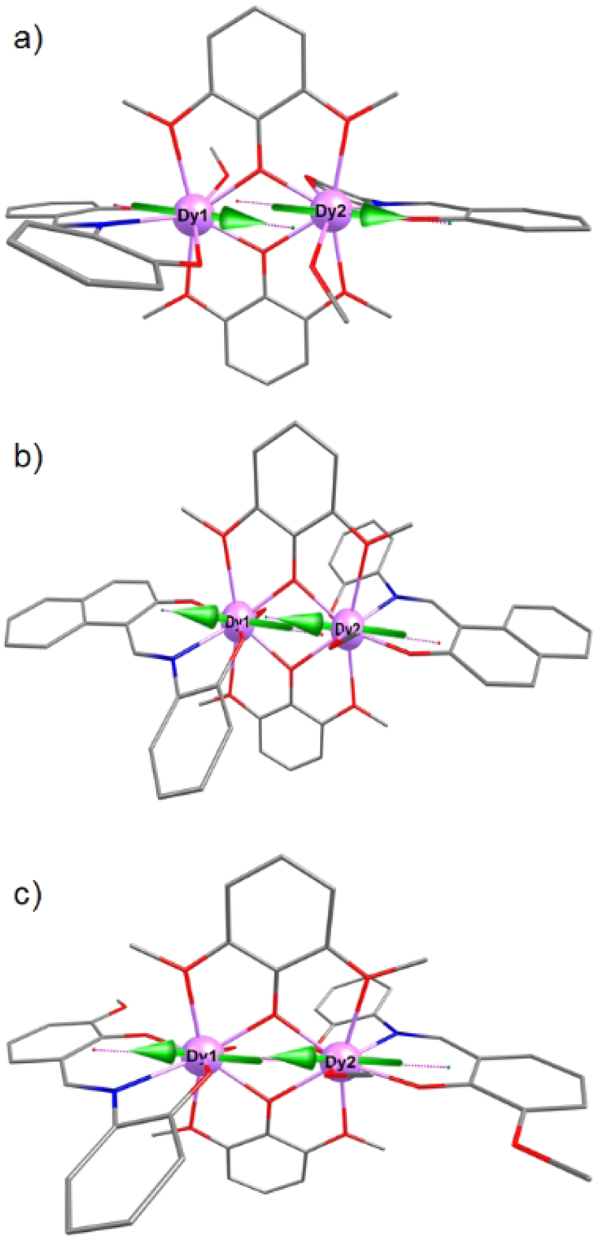

Figure 13. Orientation of the main local magnetic moment in the ground exchange doublet state of the Dy(III) ion in the complexes (a) **1a**, (b) **2a**, and (c) **3a**, where H atoms were omitted for clarity (color code Dy, pink; O, red ; N, blue ; C, gray).

observed difference in the J value for the Gd dimers, while CASSCF/RASSI-SO calculations rationalize the observed difference in the magnetization blockade and highlight how small structural differences fine-tuned by varying the ligand architecture alter the tunnelling splitting and hence the magnetization blockade.

■ ASSOCIATED CONTENT

Supporting Information

The Supporting Information is available free of charge on the ACS Publications website at DOI: 10.1021/acs.inorgchem.6b01863.

NMR and Fourier transform IR spectra, thermogravimetric analysis data, simulated and experimental powder X-ray diffraction patterns, tabulated crystal data and refinement parameters, plots of measured and calculated magnetic susceptibility with temperature, spin density plots, computed spin density values, temperature-dependent ac susceptibility, reduced magnetization versus H/T, illustrated coordination modes of ligands, calculated J values, tabulated energies of spin-free and spin-orbit states, tabulated results of ab initio calculations, computed crystal field parameters, crystal field Hamiltonian parameter, computed anisotropic g-tensor values, SHAPE measures. (PDF)

X-ray crystallographic data (CIF)

X-ray crystallographic data (CIF)

X-ray crystallographic data (CIF)

X-ray crystallographic data (CIF)

X-ray crystallographic data (CIF)

X-ray crystallographic data (CIF)

■ AUTHOR INFORMATION

Corresponding Authors

*E-mail: rajaraman@chem.iitb.ac.in. (G.R.)

*E-mail: tang@ciac.ac.cn. (J.T.)

*E-mail: sghosh@iiserpune.ac.in. Fax: +91 20 2590 8186. (S.K.G.)

Author Contributions

The manuscript was written through contributions from all authors. J.L. and G.V. contributed equally as second authors.

Notes

The authors declare no competing financial interest.

[⊥]J.L. and G.V. contributed equally as second authors.

Additional crystallographic information is available. These data can be obtained free of charge from Cambridge Crystallographic Data Centre via www.ccdc.cam.ac.uk/data_request/cif.

■ ACKNOWLEDGMENTS

S.M. is thankful to IISER Pune for research fellowship, while the research facilities provided by the same are also sincerely acknowledged. DST (Project No. GAP/DST/CHE-12-0083) is acknowledged for the financial support. DST-FIST (SR/FST/CSII-023/2012) is acknowledged for microfocus SC-XRD facility. G.R. would like to thank the DST (No. EMR/2014/000247) for funding. G.V. would like to thank Indian Institute of Technology Bombay for Post-Doctoral Fellowship.

■ REFERENCES

(1) Caneschi, A.; Gatteschi, D.; Sessoli, R.; Barra, A. L.; Brunel, L. C.; Guillot, M. Alternating current susceptibility, high field magnetization, and millimeter band EPR evidence for a ground S = 10 state in $[Mn_{12}O_{12}(Ch_3COO)_{16}(H_2O)_4].2CH_3COOH.4H_2O$. *J. Am. Chem. Soc.* **1991**, *113*, 5873−5874.

(2) Sessoli, R.; Gatteschi, D.; Caneschi, A.; Novak, M. A. Magnetic bistability in a metal-ion cluster. *Nature* **1993**, *365*, 141−143.

(3) Sessoli, R.; Tsai, H. L.; Schake, A. R.; Wang, S.; Vincent, J. B.; Folting, K.; Gatteschi, D.; Christou, G.; Hendrickson, D. N. High-spin molecules: $[Mn_{12}O_{12}(O_2CR)_{16}(H_2O)_4]$. *J. Am. Chem. Soc.* **1993**, *115*, 1804−1816.

(4) Gatteschi, D.; Caneschi, A.; Pardi, L.; Sessoli, R. Large clusters of metal ions: the transition from molecular to bulk magnets. *Science* **1994**, *265*, 1054−1058.

(5) Sessoli, R.; Powell, A. K. Strategies towards single molecule magnets based on lanthanide ions. *Coord. Chem. Rev.* **2009**, *253*, 2328−2341.

(6) Woodruff, D. N.; Winpenny, R. E. P.; Layfield, R. A. Lanthanide Single-Molecule Magnets. *Chem. Rev.* **2013**, *113*, 5110−5148.

DOI: 10.1021/acs.inorgchem.6b01863
Inorg. Chem. XXXX, XXX, XXX−XXX

(7) Giménez-Agulló, N.; de Pipaón, C. S.; Adriaenssens, L.; Filibian, M.; Martínez-Belmonte, M.; Escudero-Adán, E. C.; Carretta, P.; Ballester, P.; Galán-Mascarós, J. R. Single-Molecule-Magnet Behavior in the Family of [Ln(OETAP)$_2$] Double-Decker Complexes (Ln = Lanthanide, OETAP = Octa(ethyl)tetraazaporphyrin). *Chem. - Eur. J.* **2014**, *20*, 12817−12825.
(8) Habib, F.; Murugesu, M. Lessons learned from dinuclear lanthanide nano-magnets. *Chem. Soc. Rev.* **2013**, *42*, 3278−3288.
(9) Zhang, P.; Zhang, L.; Tang, J. Lanthanide single molecule magnets: progress and perspective. *Dalton Trans.* **2015**, *44*, 3923−3929.
(10) Zhang, P.; Guo, Y.-N.; Tang, J. Recent advances in dysprosium-based single molecule magnets: Structural overview and synthetic strategies. *Coord. Chem. Rev.* **2013**, *257*, 1728−1763.
(11) Goswami, S.; Mondal, A. K.; Konar, S. Nanoscopic molecular magnets. *Inorg. Chem. Front.* **2015**, *2*, 687−712.
(12) Christou, G.; Gatteschi, D.; Hendrickson, D. N.; Sessoli, R. Single-Molecule Magnets. *MRS Bull.* **2000**, *25*, 66−71.
(13) Chaudhari, A. K.; Joarder, B.; Rivière, E.; Rogez, G.; Ghosh, S. K. Nitrate-Bridged "Pseudo-Double-Propeller"-Type Lanthanide(III)−Copper(II) Heterometallic Clusters: Syntheses, Structures, and Magnetic Properties. *Inorg. Chem.* **2012**, *51*, 9159−9161.
(14) Luzon, J.; Sessoli, R. Lanthanides in molecular magnetism: so fascinating, so challenging. *Dalton Trans.* **2012**, *41*, 13556−13567.
(15) Chakov, N. E.; Lee, S.-C.; Harter, A. G.; Kuhns, P. L.; Reyes, A. P.; Hill, S. O.; Dalal, N. S.; Wernsdorfer, W.; Abboud, K. A.; Christou, G. The Properties of the [$Mn_{12}O_{12}(O_2CR)_{16}(H_2O)_4$] Single-Molecule Magnets in Truly Axial Symmetry: [$Mn_{12}O_{12}(O_2CCH_2Br)_{16}(H_2O)_4$]·$4CH_2Cl_2$. *J. Am. Chem. Soc.* **2006**, *128*, 6975−6989.
(16) Leuenberger, M. N.; Loss, D. Quantum computing in molecular magnets. *Nature* **2001**, *410*, 789−793.
(17) Coronado, E.; Day, P. Magnetic Molecular Conductors. *Chem. Rev.* **2004**, *104*, 5419−5448.
(18) Ardavan, A.; Rival, O.; Morton, J. J. L.; Blundell, S. J.; Tyryshkin, A. M.; Timco, G. A.; Winpenny, R. E. P. Will Spin-Relaxation Times in Molecular Magnets Permit Quantum Information Processing? *Phys. Rev. Lett.* **2007**, *98*, 057201.
(19) Roch, N.; Florens, S.; Bouchiat, V.; Wernsdorfer, W.; Balestro, F. Quantum phase transition in a single-molecule quantum dot. *Nature* **2008**, *453*, 633−637.
(20) Bogani, L.; Wernsdorfer, W. Molecular spintronics using single-molecule magnets. *Nat. Mater.* **2008**, *7*, 179−186.
(21) Mannini, M.; Pineider, F.; Danieli, C.; Totti, F.; Sorace, L.; Sainctavit, P.; Arrio, M. A.; Otero, E.; Joly, L.; Cezar, J. C.; Cornia, A.; Sessoli, R. Quantum tunnelling of the magnetization in a monolayer of oriented single-molecule magnets. *Nature* **2010**, *468*, 417−421.
(22) Urdampilleta, M.; Nguyen, N.-V.; Cleuziou, J.-P.; Klyatskaya, S.; Ruben, M.; Wernsdorfer, W. Molecular quantum spintronics: supramolecular spin valves based on single-molecule magnets and carbon nanotubes. *Int. J. Mol. Sci.* **2011**, *12*, 6656.
(23) Rinehart, J. D.; Fang, M.; Evans, W. J.; Long, J. R. Strong exchange and magnetic blocking in N_2^{3-}-radical-bridged lanthanide complexes. *Nat. Chem.* **2011**, *3*, 538−542.
(24) Katoh, K.; Isshiki, H.; Komeda, T.; Yamashita, M. Molecular spintronics based on single-molecule magnets composed of multiple-decker phthalocyaninato terbium(III) complex. *Chem. - Asian J.* **2012**, *7*, 1154−1169.
(25) Prescimone, A.; Wolowska, J.; Rajaraman, G.; Parsons, S.; Wernsdorfer, W.; Murugesu, M.; Christou, G.; Piligkos, S.; McInnes, E. J. L.; Brechin, E. K. Studies of a linear single-molecule magnet. *Dalton Trans.* **2007**, 5282−5289.
(26) Boskovic, C.; Brechin, E. K.; Streib, W. E.; Folting, K.; Bollinger, J. C.; Hendrickson, D. N.; Christou, G. Single-Molecule Magnets: A New Family of Mn_{12} Clusters of Formula [$Mn_{12}O_8X_4$(O2CPh)$_8L_6$]. *J. Am. Chem. Soc.* **2002**, *124*, 3725−3736.
(27) Brechin, E. K.; Boskovic, C.; Wernsdorfer, W.; Yoo, J.; Yamaguchi, A.; Sañudo, E. C.; Concolino, T. R.; Rheingold, A. L.; Ishimoto, H.; Hendrickson, D. N.; Christou, G. Quantum Tunneling of Magnetization in a New $[Mn_{18}]^{2+}$ Single-Molecule Magnet with S = 13. *J. Am. Chem. Soc.* **2002**, *124*, 9710−9711.
(28) King, P.; Wernsdorfer, W.; Abboud, K. A.; Christou, G. A Family of Mn_{16} Single-Molecule Magnets from a Reductive Aggregation Route. *Inorg. Chem.* **2004**, *43*, 7315−7323.
(29) Zheng, Y.-Z.; Xue, W.; Zhang, W.-X.; Tong, M.-L.; Chen, X.-M. From Pseudo to True C_3 Symmetry: Magnetic Anisotropy Enhanced by Site-Specific Ligand Substitution in Two Mn_{15}-Carboxylate Clusters. *Inorg. Chem.* **2007**, *46*, 6437−6443.
(30) Manoli, M.; Johnstone, R. D. L.; Parsons, S.; Murrie, M.; Affronte, M.; Evangelisti, M.; Brechin, E. K. A Ferromagnetic Mixed-Valent Mn Supertetrahedron: Towards Low-Temperature Magnetic Refrigeration with Molecular Clusters. *Angew. Chem., Int. Ed.* **2007**, *46*, 4456−4460.
(31) Feng, P. L.; Stephenson, C. J.; Amjad, A.; Ogawa, G.; del Barco, E.; Hendrickson, D. N. Large Spin-State Changes in Isostructural Cyanate- and Azide-Bridged $Mn_3^{III}Mn_2^{II}$ Single-Molecule Magnets. *Inorg. Chem.* **2010**, *49*, 1304−1306.
(32) Stamatatos, T. C.; Foguet-Albiol, D.; Wernsdorfer, W.; Abboud, K. A.; Christou, G. High-nuclearity, mixed-valence Mn_{17}, $Mn1_8$ and $\{Mn_{62}\}_n$ complexes from the use of triethanolamine. *Chem. Commun.* **2011**, *47*, 274−276.
(33) Nayak, S.; Evangelisti, M.; Powell, A. K.; Reedijk, J. Magnetothermal Studies of a Series of Coordination Clusters Built from Ferromagnetically Coupled $\{Mn^{II}_4Mn^{III}_6\}$ Supertetrahedral Units. *Chem. - Eur. J.* **2010**, *16*, 12865−12872.
(34) Kotzabasaki, V.; Inglis, R.; Siczek, M.; Lis, T.; Brechin, E. K.; Milios, C. J. Hexametallic manganese clusters with bulky derivatised salicylaldoximes. *Dalton Trans.* **2011**, *40*, 1693−1699.
(35) Costa, J. S.; Barrios, L. A.; Craig, G. A.; Teat, S. J.; Luis, F.; Roubeau, O.; Evangelisti, M.; Camon, A.; Aromi, G. A molecular [Mn_{14}] coordination cluster featuring two slowly relaxing nano-magnets. *Chem. Commun.* **2012**, *48*, 1413−1415.
(36) Charalambous, M.; Moushi, E. E.; Papatriantafyllopoulou, C.; Wernsdorfer, W.; Nastopoulos, V.; Christou, G.; Tasiopoulos, A. J. A $Mn_{36}Ni_4$ 'loop-of-loops-and-supertetrahedra' aggregate possessing a high $S_T = 26 \pm 1$ spin ground state. *Chem. Commun.* **2012**, *48*, 5410−5412.
(37) Chakraborty, A.; Ghosh, B. K.; Ribas-Arino, J.; Ribas, J.; Maji, T. K. A Heterometallic (Ni^{II}−Cu^{II}) Decanuclear Cluster Containing Two Distorted Cubane-like Pentanuclear Cores: Synthesis, Structure, and Magnetic Properties. *Inorg. Chem.* **2012**, *51*, 6440−6442.
(38) Nguyen, T. N.; Abboud, K. A.; Christou, G. A Mn_4 single-molecule magnet with the defective-dicubane structure from the use of pyrenecarboxylic acid. *Polyhedron* **2013**, *66*, 171−178.
(39) Nguyen, T. N.; Shiddiq, M.; Ghosh, T.; Abboud, K. A.; Hill, S.; Christou, G. Covalently Linked Dimer of Mn_3 Single-Molecule Magnets and Retention of Its Structure and Quantum Properties in Solution. *J. Am. Chem. Soc.* **2015**, *137*, 7160−7168.
(40) Zhuang, G.-M.; Li, X.-B.; Wen, Y.-Q.; Tian, C.-Y.; Gao, E.-Q. Structures and Magnetic Properties of Manganese(II) Compounds Based on Chains with Simultaneous Carboxylate and Pseudohalide Bridges. *Eur. J. Inorg. Chem.* **2014**, *2014*, 3488−3498.
(41) Piligkos, S.; Rajaraman, G.; Soler, M.; Kirchner, N.; van Slageren, J.; Bircher, R.; Parsons, S.; Güdel, H.-U.; Kortus, J.; Wernsdorfer, W.; Christou, G.; Brechin, E. K. Studies of an Enneanuclear Manganese Single-Molecule Magnet. *J. Am. Chem. Soc.* **2005**, *127*, 5572−5580.
(42) Cremades, E.; Cano, J.; Ruiz, E.; Rajaraman, G.; Milios, C. J.; Brechin, E. K. Theoretical Methods Enlighten Magnetic Properties of a Family of Mn_6 Single-Molecule Magnets. *Inorg. Chem.* **2009**, *48*, 8012−8019.
(43) Ishikawa, N.; Mizuno, Y.; Takamatsu, S.; Ishikawa, T.; Koshihara, S.-y. Effects of Chemically Induced Contraction of a Coordination Polyhedron on the Dynamical Magnetism of Bis(phthalocyaninato)disprosium, a Single-4f-Ionic Single-Molecule Magnet with a Kramers Ground State. *Inorg. Chem.* **2008**, *47*, 10217−10219.

DOI: 10.1021/acs.inorgchem.6b01863
Inorg. Chem. XXXX, XXX, XXX−XXX

(44) Milios, C. J.; Vinslava, A.; Wernsdorfer, W.; Moggach, S.; Parsons, S.; Perlepes, S. P.; Christou, G.; Brechin, E. K. A Record Anisotropy Barrier for a Single-Molecule Magnet. *J. Am. Chem. Soc.* **2007**, *129*, 2754−2755.
(45) Yoshihara, D.; Karasawa, S.; Koga, N. Cyclic Single-Molecule Magnet in Heterospin System. *J. Am. Chem. Soc.* **2008**, *130*, 10460−10461.
(46) Magnani, N.; Colineau, E.; Eloirdi, R.; Griveau, J. C.; Caciuffo, R.; Cornet, S. M.; May, I.; Sharrad, C. A.; Collison, D.; Winpenny, R. E. P. Superexchange Coupling and Slow Magnetic Relaxation in a Transuranium Polymetallic Complex. *Phys. Rev. Lett.* **2010**, *104*, 197202.
(47) Hewitt, I. J.; Tang, J.; Madhu, N. T.; Anson, C. E.; Lan, Y.; Luzon, J.; Etienne, M.; Sessoli, R.; Powell, A. K. Coupling Dy_3 Triangles Enhances Their Slow Magnetic Relaxation. *Angew. Chem., Int. Ed.* **2010**, *49*, 6352−6356.
(48) Jiang, S.-D.; Wang, B.-W.; Sun, H.-L.; Wang, Z.-M.; Gao, S. An Organometallic Single-Ion Magnet. *J. Am. Chem. Soc.* **2011**, *133*, 4730−4733.
(49) Watanabe, A.; Yamashita, A.; Nakano, M.; Yamamura, T.; Kajiwara, T. Multi-Path Magnetic Relaxation of Mono-Dysprosium-(III) Single-Molecule Magnet with Extremely High Barrier. *Chem. - Eur. J.* **2011**, *17*, 7428−7432.
(50) Gonidec, M.; Luis, F.; Vílchez, À.; Esquena, J.; Amabilino, D. B.; Veciana, J. A Liquid-Crystalline Single-Molecule Magnet with Variable Magnetic Properties. *Angew. Chem., Int. Ed.* **2010**, *49*, 1623−1626.
(51) Rinehart, J. D.; Long, J. R. Exploiting single-ion anisotropy in the design of f-element single-molecule magnets. *Chem. Sci.* **2011**, *2*, 2078−2085.
(52) Peng, G.; Mereacre, V.; Kostakis, G. E.; Wolny, J. A.; Schünemann, V.; Powell, A. K. Enhancement of Spin Relaxation in an $FeDy_2Fe$ Coordination Cluster by Magnetic Fields. *Chem. - Eur. J.* **2014**, *20*, 12381−12384.
(53) Mondal, K. C.; Sundt, A.; Lan, Y.; Kostakis, G. E.; Waldmann, O.; Ungur, L.; Chibotaru, L. F.; Anson, C. E.; Powell, A. K. Coexistence of Distinct Single-Ion and Exchange-Based Mechanisms for Blocking of Magnetization in a $Co^{II}_2Dy^{III}_2$ Single-Molecule Magnet. *Angew. Chem., Int. Ed.* **2012**, *51*, 7550−7554.
(54) Loukopoulos, E.; Berkoff, B.; Abdul-Sada, A.; Tizzard, G. J.; Coles, S. J.; Escuer, A.; Kostakis, G. E. A Disk-Like $Co^{II}_3Dy^{III}_4$ Coordination Cluster Exhibiting Single Molecule Magnet Behavior. *Eur. J. Inorg. Chem.* **2015**, *2015*, 2646−2649.
(55) Schmidt, S.; Prodius, D.; Mereacre, V.; Kostakis, G. E.; Powell, A. K. Unprecedented chemical transformation: crystallographic evidence for 1,1,2,2-tetrahydroxyethane captured within an Fe_6Dy_3 single molecule magnet. *Chem. Commun.* **2013**, *49*, 1696−1698.
(56) Joarder, B.; Chaudhari, A. K.; Rogez, G.; Ghosh, S. K. A carboxylate-based dinuclear dysprosium(III) cluster exhibiting slow magnetic relaxation behaviour. *Dalton Trans.* **2012**, *41*, 7695−7699.
(57) Mukherjee, S.; Chaudhari, A. K.; Xue, S.; Tang, J.; Ghosh, S. K. An asymmetrically connected hexanuclear Dy^{III}_6 cluster exhibiting slow magnetic relaxation. *Inorg. Chem. Commun.* **2013**, *35*, 144−148.
(58) Joarder, B.; Mukherjee, S.; Patil, M.; Xue, S.; Tang, J.; Ghosh, S. K. Chiral biomolecule based dodecanuclear dysprosium(III)−copper-(II) clusters: structural analyses and magnetic properties. *Inorg. Chem. Front.* **2015**, *2*, 854−859.
(59) Sheikh, J. A.; Goswami, S.; Konar, S. Modulating the magnetic properties by structural modification in a family of Co-Ln (Ln = Gd, Dy) molecular aggregates. *Dalton Trans.* **2014**, *43*, 14577−14585.
(60) Mondal, A. K.; Goswami, S.; Konar, S. Influence of the coordination environment on slow magnetic relaxation and photo-luminescence behavior in two mononuclear dysprosium(III) based single molecule magnets. *Dalton Trans.* **2015**, *44*, 5086−5094.
(61) Langley, S. K.; Chilton, N. F.; Ungur, L.; Moubaraki, B.; Chibotaru, L. F.; Murray, K. S. Heterometallic Tetranuclear $[Ln^{III}_2Co^{III}_2]$ Complexes Including Suppression of Quantum Tunneling of Magnetization in the $[Dy^{III}_2Co^{III}_2]$ Single Molecule Magnet. *Inorg. Chem.* **2012**, *51*, 11873−11881.
(62) Xue, S.; Ungur, L.; Guo, Y.-N.; Tang, J.; Chibotaru, L. F. Field-Induced Multiple Relaxation Mechanism of $Co^{III}_2Dy^{III}$ Compound with the Dysprosium Ion in a Low-Symmetrical Environment. *Inorg. Chem.* **2014**, *53*, 12658−12663.
(63) Feltham, H. L. C.; Clérac, R.; Powell, A. K.; Brooker, S. A Tetranuclear, Macrocyclic 3d−4f Complex Showing Single-Molecule Magnet Behavior. *Inorg. Chem.* **2011**, *50*, 4232−4234.
(64) Singh, S. K.; Beg, M. F.; Rajaraman, G. Role of Magnetic Exchange Interactions in the Magnetization Relaxation of {3d−4f} Single-Molecule Magnets: A Theoretical Perspective. *Chem. - Eur. J.* **2016**, *22*, 672−680.
(65) Costes, J. P.; Titos-Padilla, S.; Oyarzabal, I.; Gupta, T.; Duhayon, C.; Rajaraman, G.; Colacio, E. Analysis of the Role of Peripheral Ligands Coordinated to Zn^{II} in Enhancing the Energy Barrier in Luminescent Linear Trinuclear Zn-Dy-Zn Single-Molecule Magnets. *Chem. - Eur. J.* **2015**, *21*, 15785−15796.
(66) Gonidec, M.; Biagi, R.; Corradini, V.; Moro, F.; De Renzi, V.; del Pennino, U.; Summa, D.; Muccioli, L.; Zannoni, C.; Amabilino, D. B.; Veciana, J. Surface Supramolecular Organization of a Terbium(III) Double-Decker Complex on Graphite and its Single Molecule Magnet Behavior. *J. Am. Chem. Soc.* **2011**, *133*, 6603−6612.
(67) Rinehart, J. D.; Fang, M.; Evans, W. J.; Long, J. R. A N_2^{3-} Radical-Bridged Terbium Complex Exhibiting Magnetic Hysteresis at 14 K. *J. Am. Chem. Soc.* **2011**, *133*, 14236−14239.
(68) Ungur, L.; Le Roy, J. J.; Korobkov, I.; Murugesu, M.; Chibotaru, L. F. Fine-tuning the Local Symmetry to Attain Record Blocking Temperature and Magnetic Remanence in a Single-Ion Magnet. *Angew. Chem., Int. Ed.* **2014**, *53*, 4413−4417.
(69) Benelli, C.; Gatteschi, D. Magnetism of Lanthanides in Molecular Materials with Transition-Metal Ions and Organic Radicals. *Chem. Rev.* **2002**, *102*, 2369−2388.
(70) Osa, S.; Kido, T.; Matsumoto, N.; Re, N.; Pochaba, A.; Mrozinski, J. A Tetranuclear 3d−4f Single Molecule Magnet: $[Cu^{II}LTb^{III}(hfac)_2]_2$. *J. Am. Chem. Soc.* **2004**, *126*, 420−421.
(71) Palii, A.; Tsukerblat, B.; Klokishner, S.; Dunbar, K. R.; Clemente-Juan, J. M.; Coronado, E. Beyond the spin model: exchange coupling in molecular magnets with unquenched orbital angular momenta. *Chem. Soc. Rev.* **2011**, *40*, 3130−3156.
(72) Xue, S.; Chen, X.-H.; Zhao, L.; Guo, Y.-N.; Tang, J. Two Bulky-Decorated Triangular Dysprosium Aggregates Conserving Vortex-Spin Structure. *Inorg. Chem.* **2012**, *51*, 13264−13270.
(73) Guo, Y.-N.; Xu, G.-F.; Guo, Y.; Tang, J. Relaxation dynamics of dysprosium(III) single molecule magnets. *Dalton Trans.* **2011**, *40*, 9953−9963.
(74) Jiang, S.-D.; Wang, B.-W.; Su, G.; Wang, Z.-M.; Gao, S. A Mononuclear Dysprosium Complex Featuring Single-Molecule-Magnet Behavior. *Angew. Chem., Int. Ed.* **2010**, *49*, 7448−7451.
(75) Chen, G.-J.; Guo, Y.-N.; Tian, J.-L.; Tang, J.; Gu, W.; Liu, X.; Yan, S.-P.; Cheng, P.; Liao, D.-Z. Enhancing Anisotropy Barriers of Dysprosium(III) Single-Ion Magnets. *Chem. - Eur. J.* **2012**, *18*, 2484−2487.
(76) Hewitt, I. J.; Lan, Y.; Anson, C. E.; Luzon, J.; Sessoli, R.; Powell, A. K. Opening up a dysprosium triangle by ligand oximation. *Chem. Commun.* **2009**, 6765−6767.
(77) Zangana, K. H.; Moreno Pineda, E.; Winpenny, R. E. P. Single molecule magnet behaviour in a $\{Dy_4P_2\}$ octahedron. *Dalton Trans.* **2015**, *44*, 12522−12525.
(78) Guo, P.-H.; Liu, J.; Wu, Z.-H.; Yan, H.; Chen, Y.-C.; Jia, J.-H.; Tong, M.-L. Single-Molecule-Magnet Behavior in a $[2 \times 2]$ Grid Dy^{III}_4 Cluster and a Dysprosium-Doped Y^{III}_4 Cluster. *Inorg. Chem.* **2015**, *54*, 8087−8092.
(79) Chandrasekhar, V.; Das, S.; Dey, A.; Hossain, S.; Sutter, J.-P. Tetranuclear Lanthanide (III) Complexes Containing Dimeric Subunits: Single-Molecule Magnet Behavior for the Dy_4 Analogue. *Inorg. Chem.* **2013**, *52*, 11956−11965.
(80) Das, S.; Hossain, S.; Dey, A.; Biswas, S.; Sutter, J.-P.; Chandrasekhar, V. Molecular Magnets Based on Homometallic Hexanuclear Lanthanide(III) Complexes. *Inorg. Chem.* **2014**, *53*, 5020−5028.

DOI: 10.1021/acs.inorgchem.6b01863
Inorg. Chem. XXXX, XXX, XXX−XXX

(81) Goura, J.; Walsh, J. P. S.; Tuna, F.; Chandrasekhar, V. Tetranuclear Lanthanide(III) Complexes in a Seesaw Geometry: Synthesis, Structure, and Magnetism. *Inorg. Chem.* **2014**, *53*, 3385−3391.
(82) Gupta, S. K.; Rajeshkumar, T.; Rajaraman, G.; Murugavel, R. An unprecedented zero field neodymium(III) single-ion magnet based on a phosphonic diamide. *Chem. Commun.* **2016**, *52*, 7168−7171.
(83) Gupta, S. K.; Rajeshkumar, T.; Rajaraman, G.; Murugavel, R. An air-stable Dy(III) single-ion magnet with high anisotropy barrier and blocking temperature. *Chem. Sci.* **2016**, *7*, 5181−5191.
(84) AlDamen, M. A.; Clemente-Juan, J. M.; Coronado, E.; Martí-Gastaldo, C.; Gaita-Ariño, A. Mononuclear Lanthanide Single-Molecule Magnets Based on Polyoxometalates. *J. Am. Chem. Soc.* **2008**, *130*, 8874−8875.
(85) Pointillart, F.; Bernot, K.; Sessoli, R.; Gatteschi, D. Effects of 3d−4f Magnetic Exchange Interactions on the Dynamics of the Magnetization of Dy^{III}-M^{II}-Dy^{III} Trinuclear Clusters. *Chem. - Eur. J.* **2007**, *13*, 1602−1609.
(86) Ishikawa, N.; Sugita, M.; Wernsdorfer, W. Nuclear Spin Driven Quantum Tunneling of Magnetization in a New Lanthanide Single-Molecule Magnet: Bis(Phthalocyaninato)holmium Anion. *J. Am. Chem. Soc.* **2005**, *127*, 3650−3651.
(87) Ishikawa, N.; Sugita, M.; Wernsdorfer, W. Quantum Tunneling of Magnetization in Lanthanide Single-Molecule Magnets: Bis(phthalocyaninato)terbium and Bis(phthalocyaninato)dysprosium Anions. *Angew. Chem., Int. Ed.* **2005**, *44*, 2931−2935.
(88) Leng, J.-D.; Liu, J.-L.; Zheng, Y.-Z.; Ungur, L.; Chibotaru, L. F.; Guo, F.-S.; Tong, M.-L. Relaxations in heterolanthanide dinuclear single-molecule magnets. *Chem. Commun.* **2013**, *49*, 158−160.
(89) Leng, J.-D.; Liu, J.-L.; Lin, W.-Q.; Gómez-Coca, S.; Aravena, D.; Ruiz, E.; Tong, M.-L. Unprecedented ferromagnetic dipolar interaction in a dinuclear holmium(III) complex: a combined experimental and theoretical study. *Chem. Commun.* **2013**, *49*, 9341−9343.
(90) Guo, F.-S.; Liu, J.-L.; Leng, J.-D.; Meng, Z.-S.; Lin, Z.-J.; Tong, M.-L.; Gao, S.; Ungur, L.; Chibotaru, L. F. Pure Trinuclear 4 f Single-Molecule Magnets: Synthesis, Structures, Magnetism and Ab Initio Investigation. *Chem. - Eur. J.* **2011**, *17*, 2458−2466.
(91) Pedersen, K. S.; Dreiser, J.; Weihe, H.; Sibille, R.; Johannesen, H. V.; Sørensen, M. A.; Nielsen, B. E.; Sigrist, M.; Mutka, H.; Rols, S.; Bendix, J.; Piligkos, S. Design of Single-Molecule Magnets: Insufficiency of the Anisotropy Barrier as the Sole Criterion. *Inorg. Chem.* **2015**, *54*, 7600−7606.
(92) Pedersen, K. S.; Woodruff, D. N.; Bendix, J.; Clérac, R. Experimental Aspects of Lanthanide Single-Molecule Magnet Physics. In *Lanthanides and Actinides in Molecular Magnetism;* Wiley-VCH Verlag GmbH & Co. KGaA, 2015; pp 125−152.
(93) Pedersen, K. S.; Bendix, J.; Clerac, R. Single-molecule magnet engineering: building-block approaches. *Chem. Commun.* **2014**, *50*, 4396−4415.
(94) Feltham, H. L. C.; Lan, Y.; Klöwer, F.; Ungur, L.; Chibotaru, L. F.; Powell, A. K.; Brooker, S. A Non-sandwiched Macrocyclic Monolanthanide Single-Molecule Magnet: The Key Role of Axiality. *Chem. - Eur. J.* **2011**, *17*, 4362−4365.
(95) Miao, Y.-L.; Liu, J.-L.; Li, J.-Y.; Leng, J.-D.; Ou, Y.-C.; Tong, M.-L. Two novel Dy_8 and Dy_{11} clusters with cubane $[Dy_4(\mu_3\text{-}OH)_4]^{8+}$ units exhibiting slow magnetic relaxation behaviour. *Dalton Trans.* **2011**, *40*, 10229−10236.
(96) Sakaue, S.; Fuyuhiro, A.; Fukuda, T.; Ishikawa, N. Dinuclear single-molecule magnets with porphyrin−phthalocyanine mixed triple-decker ligand systems giving SAP and SP coordination polyhedra. *Chem. Commun.* **2012**, *48*, 5337−5339.
(97) Mei, X.-L.; Liu, R.-N.; Wang, C.; Yang, P.-P.; Li, L.-C.; Liao, D.-Z. Modulating spin dynamics of cyclic Ln^{III}-radical complexes (Ln^{III} = Tb, Dy) by using phenyltrifluoroacetylacetonate coligand. *Dalton Trans.* **2012**, *41*, 2904−2909.
(98) Xu, G.-F.; Wang, Q.-L.; Gamez, P.; Ma, Y.; Clerac, R.; Tang, J.; Yan, S.-P.; Cheng, P.; Liao, D.-Z. A promising new route towards single-molecule magnets based on the oxalate ligand. *Chem. Commun.* **2010**, *46*, 1506−1508.
(99) Langley, S. K.; Wielechowski, D. P.; Vieru, V.; Chilton, N. F.; Moubaraki, B.; Abrahams, B. F.; Chibotaru, L. F.; Murray, K. S. A $\{Cr^{III}_2Dy^{III}_2\}$ Single-Molecule Magnet: Enhancing the Blocking Temperature through 3d Magnetic Exchange. *Angew. Chem., Int. Ed.* **2013**, *52*, 12014−12019.
(100) Bi, Y.; Guo, Y.-N.; Zhao, L.; Guo, Y.; Lin, S.-Y.; Jiang, S.-D.; Tang, J.; Wang, B.-W.; Gao, S. Capping Ligand Perturbed Slow Magnetic Relaxation in Dysprosium Single-Ion Magnets. *Chem. - Eur. J.* **2011**, *17*, 12476−12481.
(101) Habib, F.; Brunet, G.; Vieru, V.; Korobkov, I.; Chibotaru, L. F.; Murugesu, M. Significant Enhancement of Energy Barriers in Dinuclear Dysprosium Single-Molecule Magnets Through Electron-Withdrawing Effects. *J. Am. Chem. Soc.* **2013**, *135*, 13242−13245.
(102) Langley, S. K.; Wielechowski, D. P.; Vieru, V.; Chilton, N. F.; Moubaraki, B.; Chibotaru, L. F.; Murray, K. S. Modulation of slow magnetic relaxation by tuning magnetic exchange in $\{Cr_2Dy_2\}$ single molecule magnets. *Chem. Sci.* **2014**, *5*, 3246−3256.
(103) Guo, Y.-N.; Chen, X.-H.; Xue, S.; Tang, J. Modulating Magnetic Dynamics of Three Dy_2 Complexes through Keto−Enol Tautomerism of the *o*-Vanillin Picolinoylhydrazone Ligand. *Inorg. Chem.* **2011**, *50*, 9705−9713.
(104) Zhang, P.; Zhang, L.; Lin, S.-Y.; Xue, S.; Tang, J. Modulating Magnetic Dynamics of Dy_2 System through the Coordination Geometry and Magnetic Interaction. *Inorg. Chem.* **2013**, *52*, 4587−4592.
(105) Joarder, B.; Mukherjee, S.; Xue, S.; Tang, J.; Ghosh, S. K. Structures and Magnetic Properties of Two Analogous Dy_6 Wheels with Electron-Donation and -Withdrawal Effects. *Inorg. Chem.* **2014**, *53*, 7554−7560.
(106) Zhang, L.; Zhang, P.; Zhao, L.; Wu, J.; Guo, M.; Tang, J. Anions Influence the Relaxation Dynamics of Mono-μ_3-OH-Capped Triangular Dysprosium Aggregates. *Inorg. Chem.* **2015**, *54*, 5571−5578.
(107) Wang, H.; Ke, H.; Lin, S.-Y.; Guo, Y.; Zhao, L.; Tang, J.; Li, Y.-H. Heterometallic octanuclear $RE^{III}_3Ni^{II}_5$ (RE = Dy^{III}, Gd^{III} and Y^{III}) clusters with slow magnetic relaxation for the dysprosium derivative. *Dalton Trans.* **2013**, *42*, 5298−5303.
(108) Zhang, L.; Zhang, P.; Zhao, L.; Lin, S.-Y.; Xue, S.; Tang, J.; Liu, Z. Two Locally Chiral Dysprosium Compounds with Salen-Type Ligands That Show Slow Magnetic Relaxation Behavior. *Eur. J. Inorg. Chem.* **2013**, *2013*, 1351−1357.
(109) Tian, H.; Wang, M.; Zhao, L.; Guo, Y.-N.; Guo, Y.; Tang, J.; Liu, Z. A Discrete Dysprosium Trigonal Prism Showing Single-Molecule Magnet Behaviour. *Chem. - Eur. J.* **2012**, *18*, 442−445.
(110) Mondal, K. C.; Kostakis, G. E.; Lan, Y.; Wernsdorfer, W.; Anson, C. E.; Powell, A. K. Defect-Dicubane Ni_2Ln_2 (Ln = Dy, Tb) Single Molecule Magnets. *Inorg. Chem.* **2011**, *50*, 11604−11611.
(111) Yan, P.-F.; Lin, P.-H.; Habib, F.; Aharen, T.; Murugesu, M.; Deng, Z.-P.; Li, G.-M.; Sun, W.-B. Planar Tetranuclear Dy(III) Single-Molecule Magnet and Its Sm(III), Gd(III), and Tb(III) Analogues Encapsulated by Salen-Type and *β*-Diketonate Ligands. *Inorg. Chem.* **2011**, *50*, 7059−7065.
(112) Fatila, E. M.; Rouzières, M.; Jennings, M. C.; Lough, A. J.; Clérac, R.; Preuss, K. E. Fine-Tuning the Single-Molecule Magnet Properties of a $[Dy(III)\text{-}Radical]_2$ Pair. *J. Am. Chem. Soc.* **2013**, *135*, 9596−9599.
(113) *SAINT Plus,* v 7.03; Bruker AXS Inc; Madison, WI, 2004.
(114) Sheldrick, G. M. *SHELXTL, Reference Manual, v 5.1;* Bruker AXS; Madison, WI, 1997.
(115) Sheldrick, G. M. *Acta Crystallogr., Sect. A: Found. Crystallogr.* **2008**, *64*, 112−122.
(116) Farrugia, L. *WINGX,* v 1.80.05; University of Glasgow, 2011.
(117) Spek, A. L. *PLATON, A Multipurpose Crystallographic Tool;* Utrecht University: Utrecht, The Netherlands, 2005.
(118) Merabet-Khelassi, M.; Vriamont, N.; Aribi-Zouioueche, L.; Riant, O. Racemization of secondary alcohols catalyzed by ruthenium: application to chemoenzymatic dynamic resolution. *Tetrahedron: Asymmetry* **2011**, *22*, 1790−1796.

DOI: 10.1021/acs.inorgchem.6b01863
Inorg. Chem. XXXX, XXX, XXX−XXX

(119) Basu, U.; Pant, I.; Hussain, A.; Kondaiah, P.; Chakravarty, A. R. Iron(III) Complexes of a Pyridoxal Schiff Base for Enhanced Cellular Uptake with Selectivity and Remarkable Photocytotoxicity. *Inorg. Chem.* **2015**, *54*, 3748−3758.
(120) Kim, S.; Noh, J. Y.; Kim, K. Y.; Kim, J. H.; Kang, H. K.; Nam, S.-W.; Kim, S. H.; Park, S.; Kim, C.; Kim, J. Salicylimine-Based Fluorescent Chemosensor for Aluminum Ions and Application to Bioimaging. *Inorg. Chem.* **2012**, *51*, 3597−3602.
(121) Zhang, J.; Lin, Y.-J.; Jin, G.-X. Synthesis, Characterization, and Ethylene Polymerization of Group IV Metal Complexes with Mono-Cp and Tridentate Aryloxide or Arylsulfide Ligands. *Organometallics* **2007**, *26*, 4042−4047.
(122) Jang, Y. K.; Nam, U. C.; Kwon, H. L.; Hwang, I. H.; Kim, C. A selective colorimetric and fluorescent chemosensor based-on naphthol for detection of Al^{3+} and Cu^{2+}. *Dyes Pigm.* **2013**, *99*, 6−13.
(123) Pooransingh, N.; Pomerantseva, E.; Ebel, M.; Jantzen, S.; Rehder, D.; Polenova, T. ^{51}V Solid-State Magic Angle Spinning NMR Spectroscopy and DFT Studies of Oxovanadium(V) Complexes Mimicking the Active Site of Vanadium Haloperoxidases. *Inorg. Chem.* **2003**, *42*, 1256−1266.
(124) Kannappan, R.; Tooke, D. M.; Spek, A. L.; Reedijk, J. Separation of actinides and lanthanides: Synthesis and molecular structure of a new di-μ-phenoxo-bridged dinuclear bis(dioxouranium-(VI)) complex. *Inorg. Chim. Acta* **2006**, *359*, 334−338.
(125) K Boudreaux, E. A.; Mulay, L. N. *Theory and Applications of Molecular Paramagnetism;* John Wiley & Sons: New York, 1976.
(126) Aquilante, F.; De Vico, L.; Ferre, N.; Ghigo, G.; Malmqvist, P.-A.; Neograd y, P.; Pedersen, T. B.; Pitonak, M.; Reiher, M.; Roos, B. O.; Serrano-Andres, L.; Urban, M.; Veryazov, V.; Lindh, R. MOLCAS 7: The Next Generation. *J. Comput. Chem.* **2010**, *31*, 224−247.
(127) Veryazov, V.; Widmark, P. O.; Serrano-Andres, L.; Lindh, R.; Roos, B. O. 2MOLCAS as a development platform for quantum chemistry software. *Int. J. Quantum Chem.* **2004**, *100*, 626−635.
(128) Duncan, J. A. MOLCAS 7.2. *J. Am. Chem. Soc.* **2009**, *131*, 2416−2416.
(129) Karlström, G.; Lindh, R.; Malmqvist, P. A.; Roos, B. O.; Ryde, U.; Veryazov, V.; Widmark, P. O.; Cossi, M.; Schimmelpfennig, B.; Neograd y, P.; Seijo, L. MOLCAS: a program package for computational chemistry. *Comput. Mater. Sci.* **2003**, *28*, 222−239.
(130) Chibotaru, L. F.; Ungur, L. *The computer programs SINGLE_ANISO and POLY_ANISO;* University of Leuven, 2006.
(131) Lines, M. E. Orbital Angular Momentum in the Theory of Paramagnetic Clusters. *J. Chem. Phys.* **1971**, *55*, 2977−2984.
(132) Langley, S. K.; Wielechowski, D. P.; Vieru, V.; Chilton, N. F.; Moubaraki, B.; Chibotaru, L. F.; Murray, K. S. Modulation of slow magnetic relaxation by tuning magnetic exchange in $\{Cr_2Dy_2\}$ single molecule magnets. *Chem. Sci.* **2014**, *5*, 3246−3256.
(133) van Koningsbruggen, P. J.; Gatteschi, D.; de Graaff, R. A. G.; Haasnoot, J. G.; Reedijk, J.; Zanchini, C. Isotropic and Anisotropic Magnetic Exchange Interactions through.mu.-N1,N2 1,2,4-Triazole and.mu.-Sulfato Bridges: X-ray Crystal Structure, Magnetic Properties, and Single-Crystal EPR Study of (.mu.-4-Amino-3,5-bis(pyridin-2-yl)-1,2,4-triazole-N′,N1,N2,N″)(.mu.-sulfato-O,O′)[(sulfato-O)-aquacopper(II)]triaquacopper(II) Hydrate. *Inorg. Chem.* **1995**, *34*, 5175−5182.
(134) Langley, S. K.; Ungur, L.; Chilton, N. F.; Moubaraki, B.; Chibotaru, L. F.; Murray, K. S. Single-Molecule Magnetism in a Family of $\{Co^{III}_2Dy^{III}_2\}$ Butterfly Complexes: Effects of Ligand Replacement on the Dynamics of Magnetic Relaxation. *Inorg. Chem.* **2014**, *53*, 4303−4315.
(135) Chibotaru, L. F.; Ungur, L.; Soncini, A. The Origin of Nonmagnetic Kramers Doublets in the Ground State of Dysprosium Triangles: Evidence for a Toroidal Magnetic Moment. *Angew. Chem., Int. Ed.* **2008**, *47*, 4126−4129.
(136) Ungur, L.; Van den Heuvel, W.; Chibotaru, L. F. *Ab initio* investigation of the non-collinear magnetic structure and the lowest magnetic excitations in dysprosium triangles. *New J. Chem.* **2009**, *33*, 1224−1230.
(137) Chibotaru, L. F.; Ungur, L.; Aronica, C.; Elmoll, H.; Pilet, G.; Luneau, D. Structure, Magnetism, and Theoretical Study of a Mixed-Valence $Co^{II}_3Co^{III}_4$ Heptanuclear Wheel: Lack of SMM Behavior despite Negative Magnetic Anisotropy. *J. Am. Chem. Soc.* **2008**, *130*, 12445−12455.
(138) Becke, A. D. Density-functional thermochemistry. III. The role of exact exchange. *J. Chem. Phys.* **1993**, *98*, 5648−5652.
(139) Frisch, M. J.; Trucks, G. W.; Schlegel, H. B.; Scuseria, G. E.; Robb, M. A.; Cheeseman, J. R.; Scalmani, G.; Barone, V.; Mennucci, B.; Petersson, G. A.; Nakatsuji, H.; Caricato, M.; Li, X.; Hratchian, H. P.; Izmaylov, A. F.; Bloino, J.; Zheng, G.; Sonnenberg, J. L.; Hada, M.; Ehara, M.; Toyota, K.; Fukuda, R.; Hasegawa, J.; Ishida, M.; Nakajima, T.; Honda, Y.; Kitao, O.; Nakai, H.; Vreven, T.; Montgomery, J. A., Jr.; Peralta, J. E.; Ogliaro, F.; Bearpark, M.; Heyd, J. J.; Brothers, E.; Kudin, K. N.; Staroverov, V. N.; Kobayashi, R.; Normand, J.; Raghavachari, K.; Rendell, A.; Burant, J. C.; Iyengar, S. S.; Tomasi, J.; Cossi, M.; Rega, N.; Millam, N. J.; Klene, M.; Knox, J. E.; Cross, J. B.; Bakken, V.; Adamo, C.; Jaramillo, J.; Gomperts, R.; Stratmann, R. E.; Yazyev, O.; Austin, A. J.; Cammi, R.; Pomelli, C.; Ochterski, J. W.; Martin, R. L.; Morokuma, K.; Zakrzewski, V. G.; Voth, G. A.; Salvador, P.; Dannenberg, J. J.; Dapprich, S.; Daniels, A. D.; Farkas, Ö.; Foresman, J. B.; Ortiz, J. V.; Cioslowski, J.; Fox, D. J. *Gaussian 09,* Revision A.02; Gaussian, Inc: Wallingford, CT, 2009.
(140) Cundari, T. R.; Stevens, W. J. Effective core potential methods for the lanthanides. *J. Chem. Phys.* **1993**, *98*, 5555−5565.
(141) Schafer, A.; Huber, C.; Ahlrichs, R. Fully optimized contracted Gaussian basis sets of triple zeta valence quality for atoms Li to Kr. *J. Chem. Phys.* **1994**, *100*, 5829−5835.
(142) Rajeshkumar, T.; Singh, S. K.; Rajaraman, G. A computational perspective on magnetic coupling, magneto-structural correlations and magneto-caloric effect of a ferromagnetically coupled {GdIII−GdIII} Pair. *Polyhedron* **2013**, *52*, 1299−1305.
(143) Rajeshkumar, T.; Rajaraman, G. Is a radical bridge a route to strong exchange interactions in lanthanide complexes? A computational examination. *Chem. Commun.* **2012**, *48*, 7856−7858.
(144) Chilton, N. F.; Anderson, R. P.; Turner, L. D.; Soncini, A.; Murray, K. S. PHI: A powerful new program for the analysis of anisotropic monomeric and exchange-coupled polynuclear d- and f-block complexes. *J. Comput. Chem.* **2013**, *34*, 1164−1175.
(145) Neese, F. *WIREs Comput. Mol. Sci.* **2012**, *2*, 73−78.
(146) Noodleman, L. Valence bond description of antiferromagnetic coupling in transition metal dimers. *J. Chem. Phys.* **1981**, *74*, 5737−5743.
(147) Pantazis, D. A.; Neese, F. All-Electron Scalar Relativistic Basis Sets for the Lanthanides. *J. Chem. Theory Comput.* **2009**, *5*, 2229−2238.
(148) Van Lenthe, E.; Baerends, E. J.; Snijders, J. G. Relativistic regular two-component Hamiltonians. *J. Chem. Phys.* **1993**, *99*, 4597−4610.
(149) Douglas, M.; Kroll, N. M. Quantum electrodynamical corrections to the fine structure of helium. *Ann. Phys.* **1974**, *82*, 89−155.
(150) Llunell, M, Casanova, D, Cirera, J, Alemany, P; Alvarez, S. *SHAPE,* version 2.1; Universitat de Barcelona: Barcelona, Spain, 2013.
(151) Liu, J.-L.; Chen, Y.-C.; Zheng, Y.-Z.; Lin, W.-Q.; Ungur, L.; Wernsdorfer, W.; Chibotaru, L. F.; Tong, M.-L. Switching the anisotropy barrier of a single-ion magnet by symmetry change from quasi-D_{5h} to quasi-O_h. *Chem. Sci.* **2013**, *4*, 3310−3316.
(152) Liu, S.-S.; Xu, L.; Jiang, S.-D.; Zhang, Y.-Q.; Meng, Y.-S.; Wang, Z.; Wang, B.-W.; Zhang, W.-X.; Xi, Z.; Gao, S. Half-Sandwich Complexes of Dy^{III}: A Janus-Motif with Facile Tunability of Magnetism. *Inorg. Chem.* **2015**, *54*, 5162−5168.
(153) Chen, Y.-C.; Liu, J.-L.; Ungur, L.; Liu, J.; Li, Q.-W.; Wang, L.-F.; Ni, Z.-P.; Chibotaru, L. F.; Chen, X.-M.; Tong, M.-L. Symmetry-Supported Magnetic Blocking at 20 K in Pentagonal Bipyramidal Dy(III) Single-Ion Magnets. *J. Am. Chem. Soc.* **2016**, *138*, 2829−2837.
(154) Kahn, O. *Molecular Magnetism;* Wiley-VCH: New York, 1993.
(155) Guo, Y.-N.; Xu, G.-F.; Wernsdorfer, W.; Ungur, L.; Guo, Y.; Tang, J.; Zhang, H.-J.; Chibotaru, L. F.; Powell, A. K. Strong Axiality

DOI: 10.1021/acs.inorgchem.6b01863
Inorg. Chem. XXXX, XXX, XXX−XXX

and Ising Exchange Interaction Suppress Zero-Field Tunneling of Magnetization of an Asymmetric Dy_2 Single-Molecule Magnet. *J. Am. Chem. Soc.* **2011**, *133*, 11948−11951.
(156) Zou, L.; Zhao, L.; Chen, P.; Guo, Y.-N.; Guo, Y.; Li, Y.-H.; Tang, J. Phenoxido and alkoxido-bridged dinuclear dysprosium complexes showing single-molecule magnet behaviour. *Dalton Trans.* **2012**, *41*, 2966−2971.
(157) Tang, J.; Hewitt, I.; Madhu, N. T.; Chastanet, G.; Wernsdorfer, W.; Anson, C. E.; Benelli, C.; Sessoli, R.; Powell, A. K. Dysprosium Triangles Showing Single-Molecule Magnet Behavior of Thermally Excited Spin States. *Angew. Chem., Int. Ed.* **2006**, *45*, 1729−1733.
(158) Langley, S. K.; Chilton, N. F.; Moubaraki, B.; Murray, K. S. Single-Molecule Magnetism in Three Related $\{Co^{III}_2Dy^{III}_2\}$-Acetylacetonate Complexes with Multiple Relaxation Mechanisms. *Inorg. Chem.* **2013**, *52*, 7183−7192.
(159) Bartolome, J.; Filoti, G.; Kuncser, V.; Schinteie, G.; Mereacre, V.; Anson, C. E.; Powell, A. K.; Prodius, D.; Turta, C. Magneto-structural correlations in the tetranuclear series of $\{Fe_3LnO_2\}$ butterfly core clusters: Magnetic and Mössbauer spectroscopic study. *Phys. Rev. B: Condens. Matter Mater. Phys.* **2009**, *80*, 1−16.
(160) Luis, F.; Bartolome, J.; Fernandez, J. F.; Tejada, J.; Hernandez, J. M.; Zhang, X. X.; Ziolo, R. Thermally activated and field-tuned tunneling in Mn_{12}Ac studied by ac magnetic susceptibility. *Phys. Rev. B: Condens. Matter Mater. Phys.* **1997**, *55*, 11448−11456.
(161) Costes, J. P.; Titos-Padilla, S.; Oyarzabal, I.; Gupta, T.; Duhayon, C.; Rajaraman, G.; Colacio, E. Effect of Ligand Substitution around the Dy^{III} on the SMM Properties of Dual-Luminescent Zn−Dy and Zn−Dy−Zn Complexes with Large Anisotropy Energy Barriers: A Combined Theoretical and Experimental Magnetostructural Study. *Inorg. Chem.* **2016**, *55*, 4428−40.
(162) Wang, Y. L.; Han, C. B.; Zhang, Y. Q.; Liu, Q. Y.; Liu, C. M.; Yin, S. G. Fine-Tuning Ligand to Modulate the Magnetic Anisotropy in a Carboxylate-Bridged Dy_2 Single-Molecule Magnet System. *Inorg. Chem.* **2016**, *55*, 5578−5584.
(163) Long, J.; Habib, F.; Lin, P. H.; Korobkov, I.; Enright, G.; Ungur, L.; Wernsdorfer, W.; Chibotaru, L. F.; Murugesu, M. Single-Molecule Magnet Behavior for an Antiferromagnetically Superexchange-Coupled Dinuclear Dysprosium(III) Complex. *J. Am. Chem. Soc.* **2011**, *133*, 5319−5328.
(164) Chow, C. Y.; Bolvin, H.; Campbell, V. E.; Guillot, R.; Kampf, J. W.; Wernsdorfer, W.; Gendron, F.; Autschbach, J.; Pecoraro, V. L.; Mallah, T. Assessing the exchange coupling in binuclear lanthanide(iii) complexes and the slow relaxation of the magnetization in the antiferromagnetically coupled Dy2 derivative. *Chem. Sci.* **2015**, *6*, 4148−4159.
(165) Biswas, S.; Das, S.; Rogez, G.; Chandrasekhar, V. Hydrazone-Ligand-Based Homodinuclear Lanthanide Complexes: Synthesis, Structure, and Magnetism. *Eur. J. Inorg. Chem.* **2016**, *2016* (20), 3322−3329.
(166) Gregson, M.; Chilton, N. F.; Ariciu, A.-M.; Tuna, F.; Crowe, I. F.; Lewis, W.; Blake, A. J.; Collison, D.; McInnes, E. J. L.; Winpenny, R. E. P.; Liddle, S. T. A monometallic lanthanide bis(methanediide) single molecule magnet with a large energy barrier and complex spin relaxation behavior. *Chem. Sci.* **2016**, *7*, 155−165.
(167) Liddle, S. T.; van Slageren, J. Improving f-element single molecule magnets. *Chem. Soc. Rev.* **2015**, *44*, 6655−6669.

DOI: 10.1021/acs.inorgchem.6b01863
Inorg. Chem. XXXX, XXX, XXX−XXX